RESEARCH ARTICLE

INTERNATIONAL RESEARCH JOURNAL OF MULTIDISCIPLINARY TECHNOVATION

Asian Research Association

DOI: 10.54392/irjmt2635

Palladium (II)-Quinoxaline Complex as A Potent Antioxidant, Antimicrobial, and Antidiabetic Agent: Design, Synthesis, in Vitro and in Silico Evaluation

M. Periyannan [a], A. Selvi [a], R. Rajavel [a, *]

[a] Bio-Inorganic Chemistry Research Laboratory, Department of Chemistry, Periyar University, Salem, 636 011, Tamil Nadu, India

* Corresponding Author Email: drrajavel@periyaruniversity.ac.in

DOI: https://doi.org/10.54392/irjmt2635

Received: 05-11-2025; Revised: 27-03-2026; Accepted: 18-04-2026; Published: 06-05-2026

Abstract: A Schiff base ligand (E)-11-(2-phenylhydrazono)-11H-indeno[1,2-b] quinoxaline was synthesized by the condensation of o-phenylenediamine with ninhydrin followed by its Pd (II) complex under refluxing condition. The newly formed compounds have been systematically characterized by various spectroscopic and analytical techniques which include UV–Vis, FT-IR, ^{1}H-NMR, Mass spectroscopy; additionally supported by elemental analysis for their chemical composition. A square-planar geometry has been proposed for the Pd(II) complex. The Pd (II) complex demonstrated notable antioxidant potential in ABTS and FRAP assays. Pd(II) complex demonstrated antimicrobial activity against *Staphylococcus aureus* and *Candida albicans*. Dose-dependent α-amylase inhibition (IC_{50} = 326.47 µg/mL) exhibiting a mixed mode was observed. *In silico* studies using molecular docking indicate a binding energy of -7.65 kcal/mol and stable interactions at the α-amylase active site. Molecular dynamics simulations (100 ns) revealed structural stability of the ligand–enzyme complex. MM/GBSA free energy calculations estimated a binding free energy of −61.4 kcal/mol, dominated by van der Waals and lipophilic interactions. These findings underscore the potential of the Pd(II) complex as a promising antidiabetic and antimicrobial agent and warrant further investigation into its mechanism of action and *in vivo* efficacy.

Keywords: Pd(II) Acetate Complex, Bio-Effectiveness, Radical Scavenging, Molecular Docking.

1. Introduction

Recent years have seen significant research interest in the synthesis of Schiff base ligands containing the imine (–HC=N–) group due to their strong coordinating ability with transition metals. Owing to their easy preparation and versatile properties, these ligands are widely used in catalysis and biological studies. [1-5] Among them, quinoxaline-based Schiff bases are particularly important for their diverse pharmacological activities, including antibacterial, antifungal, antidepressant and anticancer effects. Building on earlier studies of Pd(II) acetate complexes with such ligands, current research focuses on their synthesis, characterization, and biological evaluation, along with molecular modelling investigations. In this context, the present work explores a Pd(II) Schiff base quinoxaline complex, assessing its antioxidant potential, radical scavenging ability, ferric reducing power, and antifungal, anticancer, and antidiabetic activities.

Indenoquinoxaline scaffolds are characterised by their fused nitrogen-containing heterocyclic framework which comprises of an indeno group and a quinoxaline moiety. These scaffolds have gained considerable attention due to their broad utility in synthetic and medicinal chemistry, that is as building blocks in the design of pharmaceuticals, dyes, and advanced materials [6]. These scaffolds are used in the synthesis of spiroheterocycles, a class of compounds which are known for their structural diversity and promising bioactivity. Indenoquinoxalines can also be further chemically fused with other heterocyclic systems, viz., thiazole, hydrazide, and benzimidazole rings, which are used for therapeutic potential as well as for environmental applications [7-10].

Metal complexes derived from indenoquinoxaline ligands have expanded the functional versatility of this heterocyclic framework, particularly through interactions with transition metals. [11,12]. These interactions yield a broad array of coordination structures that exhibit distinct chemical and biological behaviors. Metals such as Cu(II), Co(II), Zn(II), and Ni(II) are frequently utilized for metal-complex synthesis [13,14]. These compounds are synthesised either by direct combination of starting materials in a multicomponent fashion or by introducing metal ions into pre-assembled ligands [15-16]. Functionally, many of

these complexes display heightened bioactivity, including cytotoxic, antimicrobial, and neuroprotective effects and often outperforming the unbound ligand due to changes in membrane transport and redox potential. [17-20]. Additionally, cooperative magnetic behavior are shown by some ligand-metal complexes. Also, these complexes serve as oxidation catalysts, which suggests a broader applicability in biomedical and environmental contexts [21-23].

Schiff base compounds formed by attaching azomethine (-C=N-) groups to indenoquinoxaline structures via condensation with amines or hydrazine have drawn attention due to their chemical adaptability and biological relevance. This linkage forms when the carbonyl moiety of the indenoquinoxaline engages with nitrogen-containing nucleophiles, producing diverse products depending on the specific amine involved [24]. Many of these molecules are further modified with heterocyclic structures like thiazole rings. The resulting hybrids, which would contain the rigid fused-ring system that is combined with imine linkages and various side chains, often would show promising activity in biomedical contexts [25-26]. Their antioxidant behaviors is thought to stem from the capacity of their conjugated systems to stabilize reactive species. In addition, some variants have been found to interfere with enzymes such as α-glucosidase, pointing to possible roles in managing metabolic disorders like diabetes [8,27]. Further, antimicrobial properties of these complexes have also been reported [28]. Among these, phenylhydrazone-derived indenoquinoxaline Schiff bases are particularly noteworthy. These are synthesized via condensation of phenylhydrazone with carbonyl-functionalized indenoquinoxaline derivatives. These molecules integrate the characteristic hydrazone functionality with the indenoquinoxaline core, enhancing their chemical versatility and bioactivity [11,29].

Palladium (Pd) Schiff base complexes have emerged as a distinct class of coordination compounds with significant therapeutic and catalytic potential [30,31]. Pd in its +2 oxidation state tends to adopt a square planar shape, which, along with its electron configuration, makes it particularly suited for forming stable bonds with Schiff base ligands that donate electrons through atoms like nitrogen, oxygen, or sulfur. Unlike metals such as Cu or Zn, Pd often engages in stronger π-backdonation and exhibits higher kinetic flexibility [32,33]. Schiff base ligands play a pivotal role in modulating the reactivity and selectivity of these complexes by influencing the electron density and overall molecular architecture [34]. Biologically, Pd-Schiff base complexes have demonstrated a wide spectrum of activity, including antibacterial, antifungal, antioxidant, antimalarial, anticancer, and antidiabetic [35-38]. In addition, these complexes have been successfully employed in the development of functional materials [30, 39-41]. The dual utility of Pd-Schiff base complexes in medicinal and material chemistry underscores its application both in material science and biological science. Keeping these views, Pd(II) complex was synthesized and characterized. Further, the biological activities of the synthesized compound such as *in vitro* antioxidant, antimicrobial, and mammalian α-amylase inhibitory effect, are determined. Further *in silico* molecular docking and molecular dynamics (MD) simulation of synthesized Pd(II) complex with human α-amylase was carried out to understand the interaction of the ligand and protein. Post-MD analysis, such as root mean square deviation (RMSD), root mean square fluctuation (RMSF), principal component analysis (PCA), detailed cross correlation map (DCCM), and binding free energy [Molecular Mechanics-Generalized Born Surface Area (MM/GBSA)] were done.

2. Experimental

2.1 Materials and Instruments

MS Scientific Chemicals & Instruments provided the chemicals o-phenylenediamine, ninhydrin, and phenylhydrazone, which were used without additional purification. Standard procedures were followed in the purification and drying of the solvents. Every reaction was carried out at room temperature. Merck pre-coated plates (silica gel 60 F254) were used for TLC analysis of all reactions. These plates were either placed in an iodine chamber or exposed to intense UV light for evaluation. Unadjusted melting points were determined using the capillary tube method and an Electrothermal 9200 instrument. Utilizing a PerkinElmer FT-IR spectrometer with a scan range of 400–4000 cm^{-1}, IR spectra were acquired. With TMS serving as an internal reference, NMR spectra were captured using a Bruker DRX-400 MHz NMR instrument in DMSO-d_6 solvent. Utilizing a Maxis 10138 mass spectrometer operating at 70 eV, high-resolution mass spectra of representative compounds were acquired.

2.2. Synthesis of Quinoxaline Schiff Base

0.1784 g of ninhydrin was added concurrently with the dissolution of 0.2164 g of o-phenylenediamine in 10 mL of ethanol. For forty-five minutes, the mixture was swirled at room temperature. TLC was used to monitor the development reaction. After completion the reaction, the reaction mixture was filtered and recrystallize using hot ethanol. The quinoxaline yellow solid precipitate was obtained. After adding a few drops of glacial acetic acid to ethanol to dissolve the quinoxaline compound obtained from the Schiff base reaction, 2-hydrazinopyridine (0.1081 g) was added. For three hours, the mixture was refluxed while being constantly stirred. Using vacuum filtration, the red solid precipitate-the quinoxaline Schiff base ligand ((E)-11-(2-phenylhydrazono)-11H-indeno[1,2-b] quinoxaline was collected. Anal. Cal. $C_{21}H_{14}N_4$: C, 78.24%; H, 4.38%; N, 17.38%. Found: C, 69.51; H, 4. 23; N, 6.12 %; IR (ATR,

cm-1): 3355 (N-H); 1690, 1641 (C=O), 1606 (C=N). UV-Vis (CH_2Cl_2, λmax, nm): 265, 382 and 507. ^{1}H-NMR (400 MHz, DMSO-d6) δ ppm: 7.0-7.1 (t,1H J = 7.2 Hz, CH_{Ar}), 7.40 (t,2H J = 7.6 Hz, CH_{Ar}), 7.54-7.59 (m,3H J = 8 Hz, CH_{Ar}), 7.65-7.69 (t, 1H, J = 7.2 Hz, CH_{Ar}), 7.88-7.90 (m,2H, J = 3.2 Hz, CH_{Ar}), 7.98-7.99 (d, 1H, J = 7.6 Hz, CH_{Ar}), 8.11-8.13 (d, 1H, J = 7.2 Hz, CH_{Ar}), 8.18-8.20 (t, 1H, J = 5.6 Hz, CH_{Ar}) 8.35-8.38 (t, 1H, J = 3.6 Hz, CH_{Ar}), 12.837 (s, 1H, NH).

2.3 Synthesis of the Palladium (II)-Quinoxaline Complex

Palladium (II) acetate (0.1 mmol) and quinoxaline Schiff base ligand (0.1 mmol) were mixed in a 1:1 solvent mixture of ethanol (10 mL) and chloroform (10 mL), and the mixture was refluxed for six hours at 95 ^{o}C with stirring. Thin layer chromatography was used to monitor the progress of the reaction. At the end, the solvent was extracted using a rotatory evaporator. Using silica gel column chromatography with a 9:1 (v/v) petroleum ether to ethyl acetate ratio as the mobile phase, the resulting crude material was processed to produce a pure product. Anal.cal: $C_{26}H_{23}N_4O_4Pd$: C, 55.57%; H, 4.13%; N, 9.97%; O, 11.39%; Pd, 18.94%. MS (ESI, m/z): required 561.91, found 561.08 [M] +. IR (FT-IR, cm-1): 3048 (N-H), 1479 (C=O), 1431 (C=N). UV-Vis (CH_2Cl_2, λmax, nm): 265, 382 and 507. ^{1}H-NMR (400 MHz, DMSO-6) δ ppm: 1.96 (s, 6H, CH_3), 6.95-699 (t,1H J = 6.9 Hz, CH_{Ar}), 7.15-7.09 (t, 1H J = 7.0 Hz, CH_{Ar}), 7.48-7.39 (m,3H J = 7.4 Hz, CH_{Ar}), 7.78-7.65 (t, 3H, J = 7.6 Hz, CH_{Ar}), 7.96-7.89 (m,2H, J = 7.8 Hz, CH_{Ar}), 8.12-8.05 (m, 2H, J = 8.06 Hz, CH_{Ar}), 8.24-8.17 (t, 1H, J = 8.27 Hz, CH_{Ar}), 8.38-8.31 (t, 1H, J = 8.27 Hz, CH_{Ar}) 8.46-8.45 (d, 1H, J = 8.4 Hz, CH_{Ar}), 11.96 (s, 1H, NH) Figure 1.

2.4 In Vitro Antioxidant Assay

The ABTS scavenging and ferric reducing antioxidant power (FRAP) assay were performed following the previous method [42, 43]. ABTS (7 mM) was reacted with 2.45 mM potassium persulfate and incubated in the dark for 12-16 h to generate ABTS$^{\bullet+}$ radicals. The solution was diluted with ethanol to an absorbance of 0.70 ± 0.02 at 734 nm and equilibrated at 30 °C. For the assay, 900 µl of the ABTS solution was mixed with various concentrations of the Pd(II) complex and made up to 1 ml with ethanol. After 3 h incubation in the dark at room temperature, absorbance was measured at 734 nm. The FRAP reagent was prepared by mixing acetate buffer (300 mM), TPTZ (10 mM in 40 mM HCl), and $FeCl_3 \cdot 6H_2O$ (20 mM) in a 10:1:1 ratio and prewarmed to 37 °C. For the assay, 300 µl of FRAP reagent was mixed with various concentrations of the Pd(II) complex and the volume adjusted to 1 ml with distilled water. After 15 min incubation at 37 °C, absorbance was measured at 593 nm.

2.5 Antimicrobial Assay

The antibacterial and antifungal activity of the Pd(II) complex was evaluated against *Staphylococcus aureus* and *Candida albicans*. For the zone of inhibition (ZOI) assay, Mueller–Hinton agar (MHA) was used for *S. aureus*, while Sabouraud dextrose agar (SDA) was used for *C. albicans*. The media were prepared in distilled water (pH 7.0) and sterilized by autoclaving at 121 °C for 15 minutes. After solidification, plates were inoculated with microbial suspensions, approximately 10^6 CFU/mL using a sterile cotton swab.

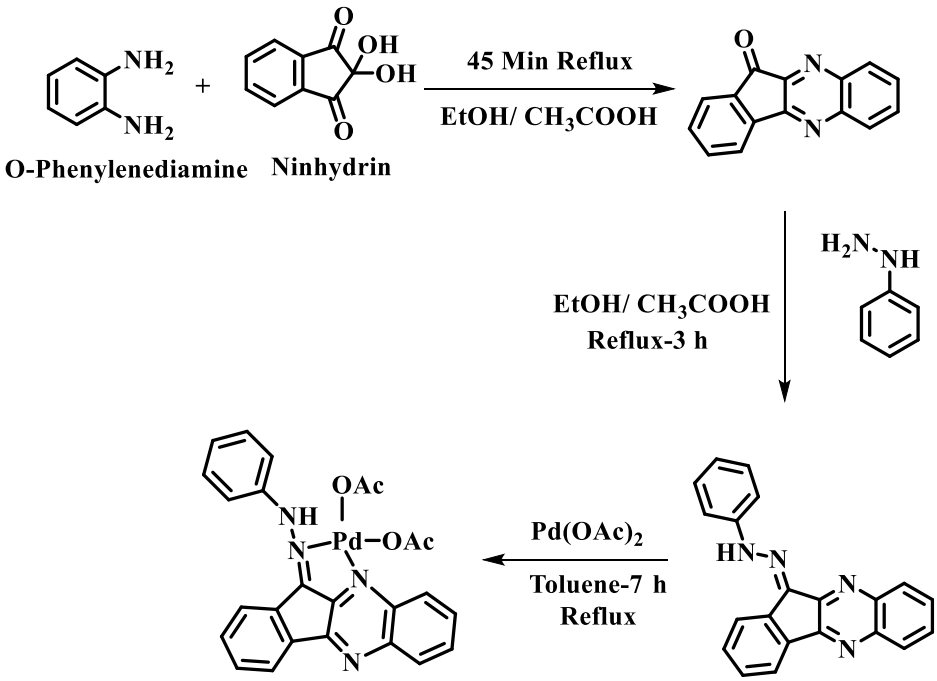

Figure 1. Synthesis of the Quinoxaline Ligand and its Pd (II) Complex

Wells of 8 mm diameter were punched into the agar, and different concentrations of the Pd(II) complex (400, 600, 800, and 1000 µg/mL) were added into respective wells. Amikacin (for *S. aureus*) and voriconazole (for *C. albicans*) were used as standard controls. The plates were allowed to stand at room temperature for 4 hours followed by incubation at 37 °C for 24 hours (for bacteria) and 30 °C for 48–72 hours (for fungi). After incubation, the diameter of the inhibition zones was measured in millimeters.

2.6 MIC, MBC and MFC Analysis

The minimum inhibitory concentration (MIC) of the Pd(II) complex was determined using the broth microdilution method. Serial dilutions of the compound were prepared in Mueller–Hinton broth for bacterial assays and Sabouraud dextrose broth for fungal assays. A standardized inoculum equivalent to 0.5 McFarland standard was diluted to achieve a final concentration of approximately 5 × 10^5 CFU/mL in each well of a sterile 96-well microtiter plate. Each well contained 190 µL of the diluted compound and 10 µL of microbial suspension. Positive controls (broth with inoculum) and negative controls (broth only) were included. The plates were incubated at 37 °C for 24 hours for *S. aureus* and 30 °C for 48 hours for *C. albicans*. The MIC was defined as the lowest concentration of the compound that completely inhibited visible microbial growth. The minimum bactericidal concentration (MBC) and minimum fungicidal concentration (MFC) were determined following the MIC assay. Aliquots (10 µL) from wells corresponding to the MIC and higher concentrations were spread onto fresh MHA (for bacteria) and SDA (for fungi) plates. The plates were incubated at 37 °C for 18–24 hours for *S. aureus* and 28–30 °C for 24–48 hours for *C. albicans*. After incubation, colony formation was assessed. The lowest concentration that resulted in no visible growth or fewer than 10 colonies (≥99.9% killing) was recorded as the MBC or MFC.

2.7 A-Amylase Inhibition Assay

The assay was conducted using porcine pancreatic α-amylase (1 mg/mL). The reaction mixture consisted of 50 µL of the enzyme and 0.1% starch in 1 mL of 20 mM potassium phosphate buffer (pH 7) and was incubated at 37 °C for 1 hour. The reaction was terminated by adding 1 mL of dinitro salicylic acid (DNS) reagent, followed by boiling for 15 minutes. After cooling, absorbance was measured at 540 nm. For inhibition studies, α-amylase was preincubated with Pd(II) complex at concentrations ranging from 100 to 500 µg/mL for 30 minutes, and residual activity was assessed as described. Enzyme kinetics were evaluated using varying starch concentrations (0.1%–0.2%), and the inhibition type and Ki values were determined using Lineweaver–Burk and Dixon plots [44].

2.8 Molecular Docking Analysis

The chemical structure of the synthesized Pd (II) complex was generated using ChemDraw, while the three-dimensional coordinates of human α-amylase were obtained from the Protein Data Bank (PDB ID: 4GQR) [45]. Prior to docking, both the ligand and protein were prepared using standard protocols in the Auto Dock suite. Docking simulations were carried out with a grid box dimension of 52 × 50 × 56, cantered at coordinates 0.45, 10.062, and -5.874, using default grid spacing settings [46]. Post-docking, the binding interactions between the metal complex and the active site residues of the enzyme were examined using PyMOL to visualize and interpret the molecular contacts involved.

2.9 Molecular Dynamics Study

Molecular dynamics (MD) simulations were conducted using the Desmond module within the Schrödinger suite, applying the OPLS4 force field [47, 48]. An orthorhombic simulation box was constructed with a 10 Å buffer using the TIP3P water model to solvate the system. Counterions (Na^+/Cl^-) were introduced uniformly to achieve overall charge neutrality and to accommodate Ewald summation requirements. Energy minimization was carried out using both steepest descent and conjugate gradient algorithms. The system was gradually heated from 0 Ks to 300 K over 200 ps under an NVT ensemble to equilibrate temperature. Following this, production runs were executed for 100 nanoseconds under NPT conditions, maintaining constant temperature (300 K) and pressure (1 bar) with a 2 fs integration time step. The dynamic stability and flexibility of the ligand–α-amylase complexes were evaluated by tracking RMSD and RMSF metrics across the simulation timeline [49, 50]. To further assess motion patterns and residue correlations, PCA and DCCM were generated using CPPTRAJ and R-based analytical tools [51, 52]. Additionally, binding free energy estimations (MM/GBSA) were performed using trajectory snapshots from the 50 ns and 100 ns marks via the Prime module integrated in the Schrödinger platform [53-55]. Visualization of the complex and analysis of key interactions were carried out using PyMOL [The Pymol Molecular Graphics System Version 2.0, Schrodinger LLC] and Discovery Studio Visualizer [BIOVIA, San Diego, CA, USA].

2.10 Statistical Analysis

All experiments were performed in triplicates, and results were expressed as mean ± standard deviation (SD). One-way ANOVA followed by Tukey's post hoc test was used to assess statistical significance, with a p-value < 0.05 considered significant. Graphical representations were generated using GraphPad Prism software.

3. Result and Discussion

3.1 Electrical Spectra

The electronic spectra of the quinoxaline ligand and its Pd(II) complex was recorded in a 10^{-5} M $CHCl_3$ solution at room temperature over the wavelength range of 200–800 nm (Figure 2). The free ligand exhibits three absorption bands at approximately 272 nm (ε = 2,50,980 M^{-1} cm^{-1}), 388 nm (ε = 1,66,180 M^{-1} cm^{-1}), and 496 nm (ε = 74,515 M^{-1} cm^{-1}), which are attributed to intra-ligand π→π* and n→π* transitions ligand moiety. In the spectra of the complexes, these transitions are observed with slight shifts in energies at 279 (ε = 2,90,000 M^{-1} cm^{-1}), 395(ε = 2,29,000 M^{-1} cm^{-1}), and 572 (ε = 31,000 M^{-1} cm^{-1}), indicating coordination of the ligand to the palladium metal ion [56].

3.2 Infrared Spectra

The infrared spectrum of Schiff base ligand shows a prominent band at 1604 cm^{-1} associated with the ν(C=N) stretching vibration and a N–H stretching band at 3355 cm^{-1}. These bands are displaced to lower wavenumbers in the palladium (II) complex, appearing at 1479 cm^{-1} and 3048 cm^{-1}, respectively, indicating that the azomethine nitrogen atom is coordinated to the metal centre [21]. An absorption band at approximately 513 cm^{-1} is associated with the ν(M–N) stretching vibration, confirming that the metal–ligand bond has formed. The Pd (II) complex showed slight changes in C–H stretching and bending frequencies in comparison to the unbound ligand. Collectively, these spectral changes support coordination through the azomethine nitrogen (Figure 3).

3.3 ^{1}H NMR Spectra of Synthesised Quinoxaline Schiff Base Ligand and Its Pd (II) Complex

The ^{1}H NMR spectra of the synthesized ligand and its corresponding palladium (II) complex provide clear evidence for coordination without deprotonation. Upon comparison of the spectra, noticeable changes in chemical shifts are observed, confirming the interaction between the ligand and the palladium centre. The NH proton signal present in the free ligand appears in the downfield region (12.84 ppm) and is retained in the palladium complex with only a slight shift, indicating that this proton is not involved in deprotonation or direct coordination. This suggests that the ligand coordinates to the metal ion in a neutral form. The aromatic protons of both the ligand and the complex resonate in the region δ 8.8–6.9 ppm, showing minor downfield shifts upon complexation due to deshielding effects arising from coordination with the palladium (II) ion. These shifts support the involvement of nearby donor atoms in binding. Additionally, the appearance of a new singlet in the region δ 1.96 ppm in the complex is attributed to the methyl protons of the coordinated acetate (OAc) groups, confirming the incorporation of the Pd $(OAc)_2$ moiety.

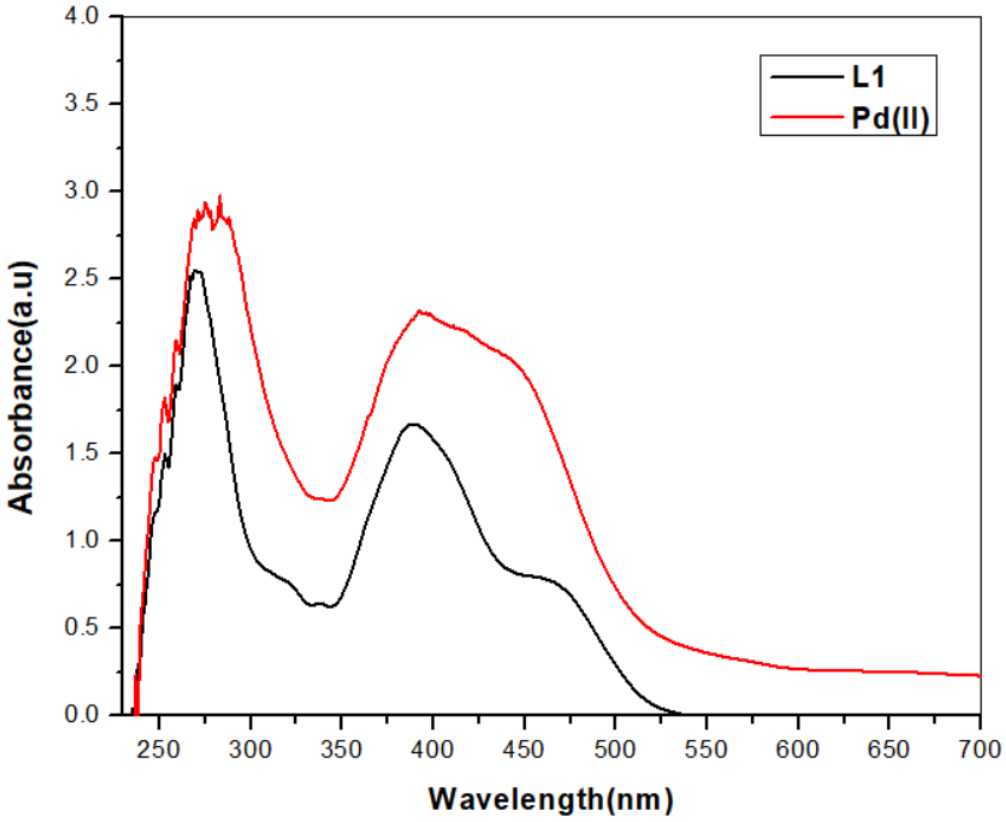

Figure 2. UV-Visible Spectra Of A) Schiff Base Ligand and B) Pd (II) Complex

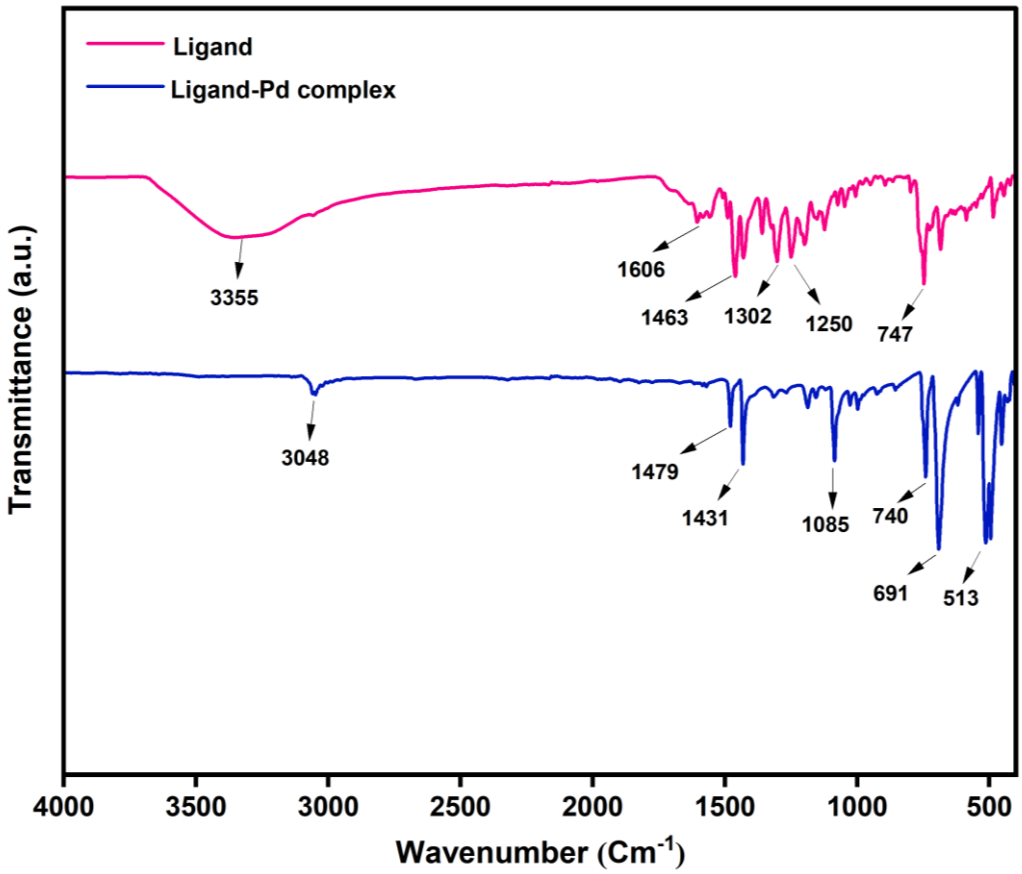

Figure 3. FTIR-Spectra of a) Quinoxaline Ligand and B) Pd (II) Complex**.**

Overall, the ^{1}H NMR spectral data indicate that coordination occurs through the azomethine nitrogen and adjacent heteroaromatic nitrogen atoms, while the NH group remains non-coordinated and intact in the complex (Figures 4, 5).

3.4 Mass Spectrometry

The base peak of the Schiff base ligand is represented by the [M + H] $^+$ ion, which is represented by a molecular ion peak at m/z 323.52. The calculated molecular weight of the ligand is 322.36 g·mol^{-1}, which is consistent with the m/z value that was found. A molecular ion peak at m/z 561.91 is visible in the mass spectrum of the pd(II) complex, confirming the proposed molecular formula. The ligand and palladium complex mass spectra are displayed in Figure 6.

3.5 XPS Study

The primary purpose of an X-ray photoelectron spectroscopy (XPS) examination of a Pd (II) complex is to verify the palladium's oxidation state and its coordination environment with ligands. For a Pd (II) system, the most important region is the Pd 3d core-level spectrum investigates typically shows two characteristic peaks due to spin-orbit splitting of Pd $3d_{3/2}$ and Pd $3d_{5/2}$ the peak appears at the binding energies of 341.15 eV and 335.78 respectively. The separation between these peaks is approximately 5.37 eV, confirming these binding energies are characteristic of Pd in +2 oxidation state. In addition, pd with complementary shifts in ligand-associated peaks N 1s, O 1s and C 1s further verify strong metal-ligand interactions and the formation of a well-defined Pd (II) coordination complex. The O 1s spectrum can be deconvoluted into multiple components corresponding to lattice oxygen, surface hydroxyl groups, and adsorbed oxygen species. The dominant peak at ~531.21 and ~532.64 eV is attributed to lattice oxygen (Pd-O-Pd), confirming the formation of palladium oxide or strong Pd-O bonding. Additional peaks at higher binding energies ~533.96 arise from surface hydroxyl groups and adsorbed oxygen species, indicating the presence of defect sites and surface functionalization. Concurrently, the Pd 3d spectrum exhibits a positive shift relative to metallic Pd, further supporting the electron-withdrawing effect of oxygen and the stabilization of Pd in the +2-oxidation state. These results collectively confirm the successful formation of Pd–O interactions with significant surface reactivity. The peak at ~398.5 eV is assigned to uncoordinated nitrogen species, while the shifted peak at ~400.5 eV is attributed to nitrogen atoms coordinated with Pd, confirming the formation of Pd-N bonds. This positive shift in binding energy arises from electron donation from nitrogen to Pd, resulting in reduced electron density around nitrogen.

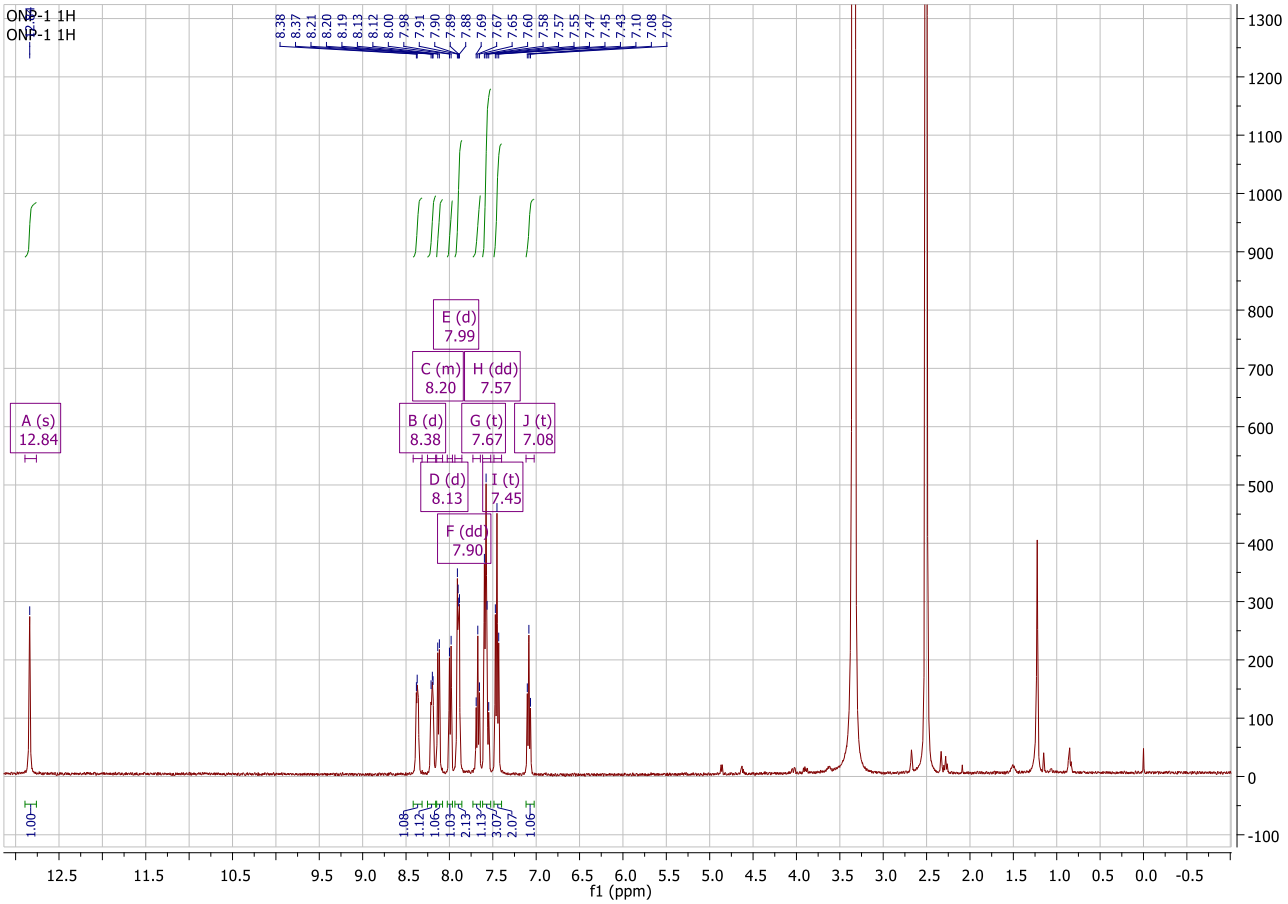

Figure 4. [1]HNMR-Spectra Quinoxaline Schiff Base Ligand

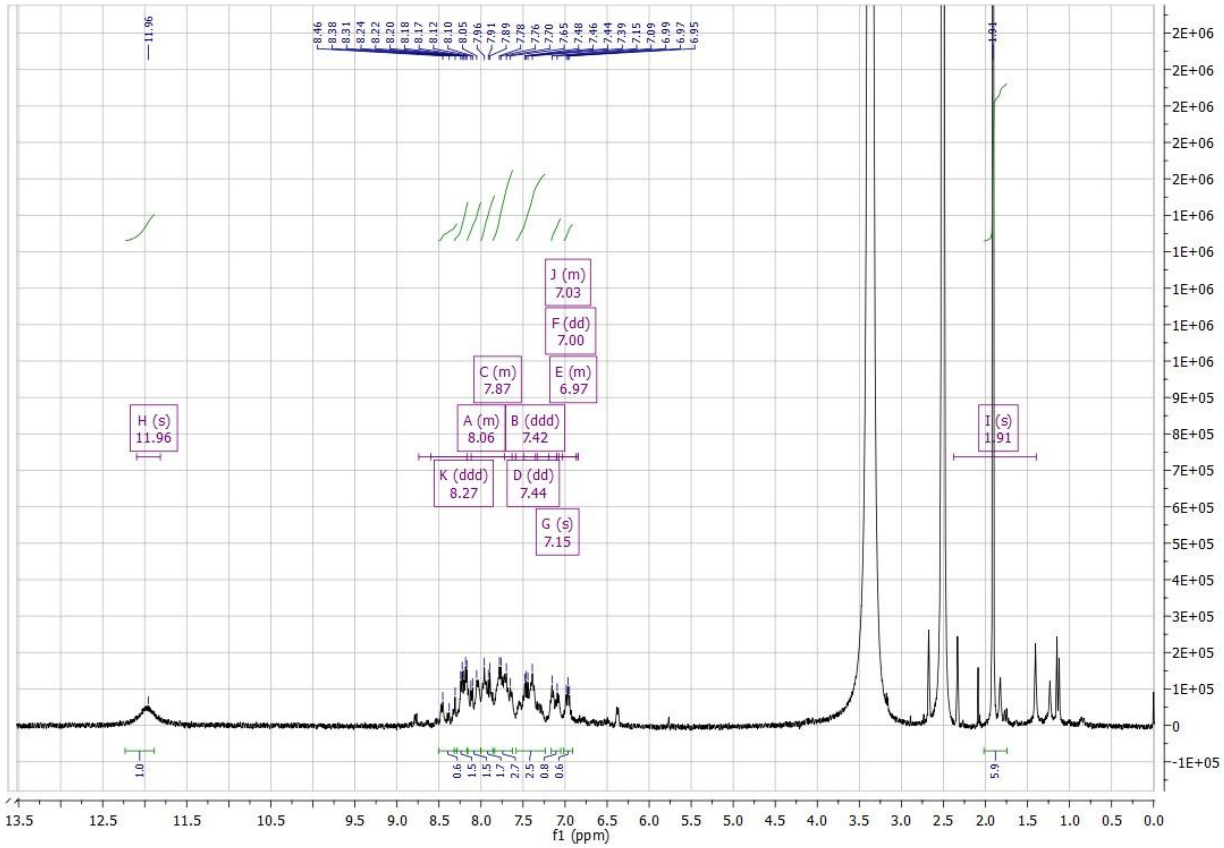

Figure 5. [1]H NMR—Spectra of Pd (II) complex

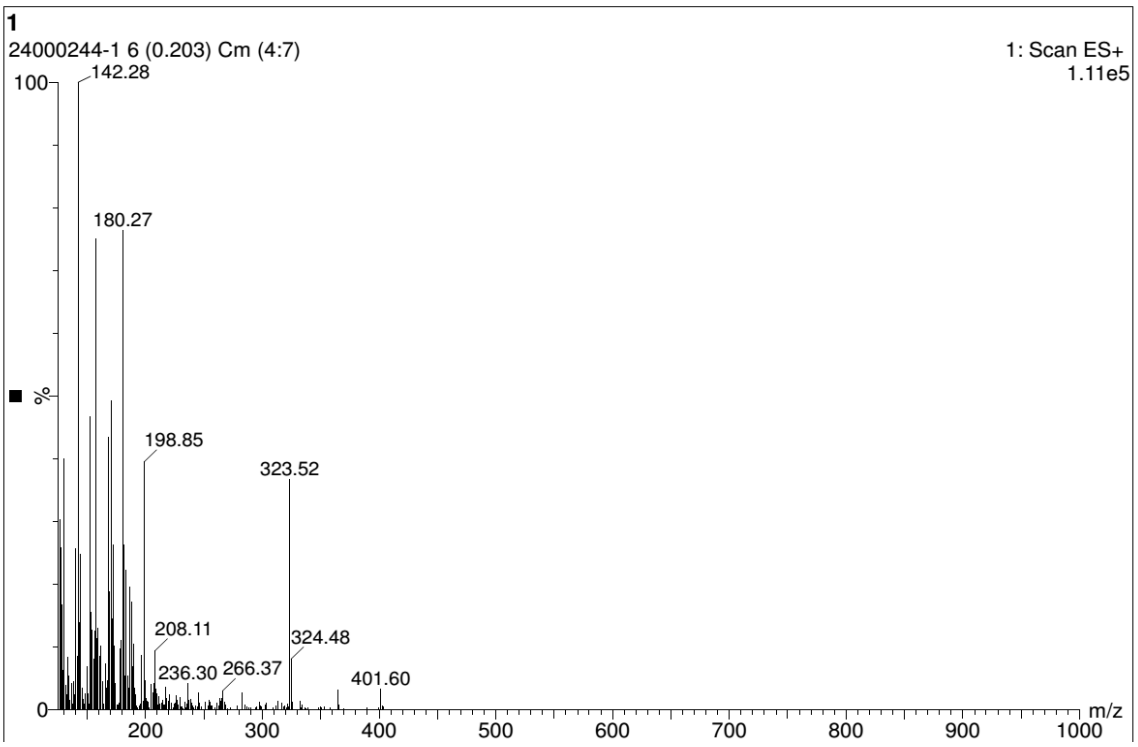

Figure 6. Mass-Spectr

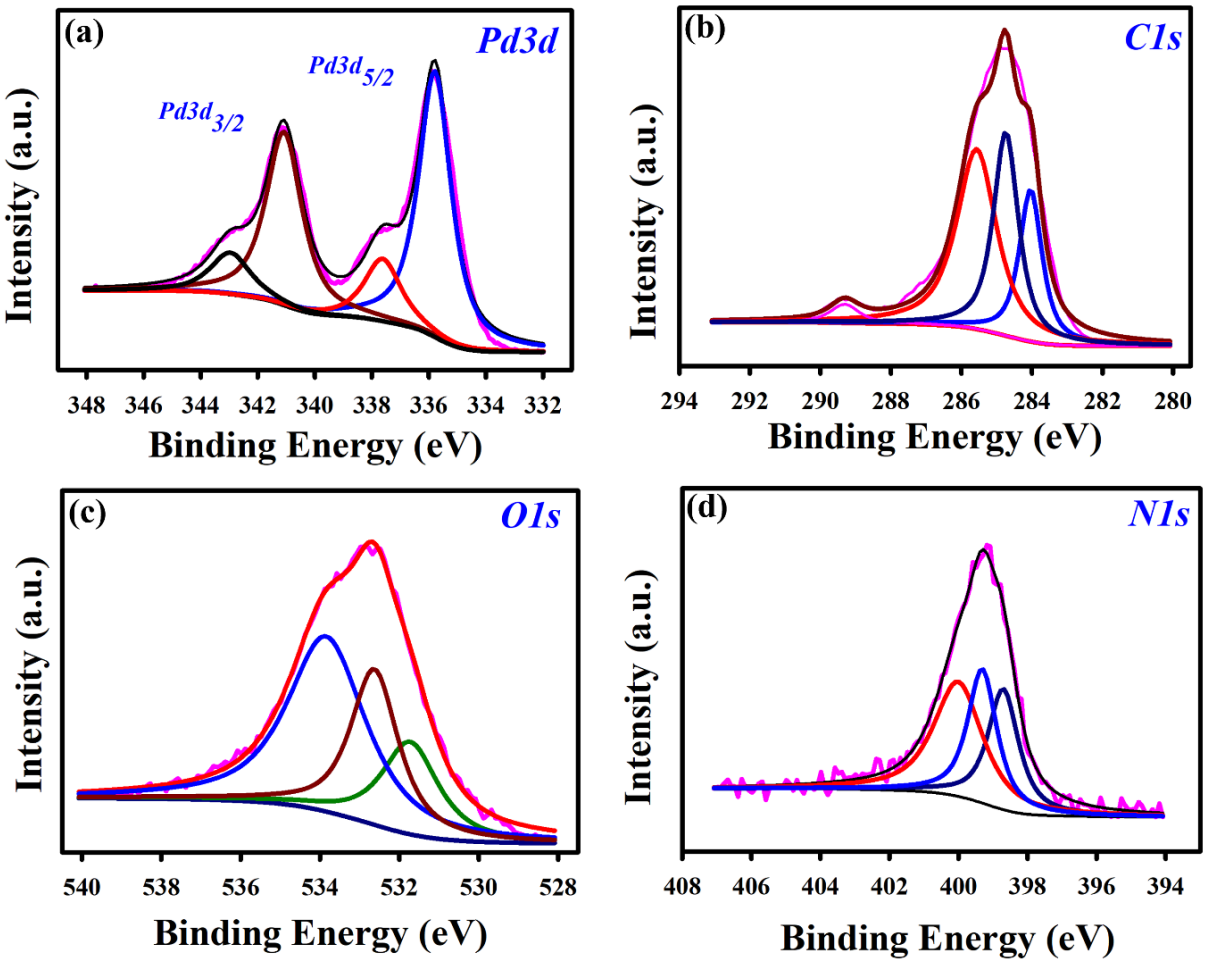

Figure 7. XPS spectra of Pd (II) Complex exhibited **(a)** Pd3d, **(b)** C1s, **(c)** O1s **(d)** N1s

3.6 Antioxidant Activity of the Pd (II) Complex

The antioxidant activity of the synthesized Pd (II) complex was evaluated using two assays: ABTS radical scavenging activity and the FRAP assay. In the ABTS assay, the complex exhibited a concentration-dependent increase in radical scavenging activity. The scavenging activity increased from 15.7% at 30 µg/mL to 83.7% at 150 µg/mL concentrations (Figure 8A). The IC_{50} value of the complex was determined to be 130.5 µg/mL, indicating moderate antioxidant potential. In comparison, the standard antioxidant ascorbic acid showed significantly higher activity with an IC_{50} value of 2.79 µg/mL (Figure 8B). In the FRAP assay, the Pd (II) complex also demonstrated a dose-dependent increase in reducing power. The optical density (OD) values at 593 nm increased from 0.142 at 30 µg/mL to 0.438 at 150 µg/mL (Figure 8C). These values reflect the compound's ability to reduce Fe^{3+} to Fe^{2+}, confirming its antioxidant capacity. However, the standard ascorbic acid displayed higher reducing power across all tested concentrations, with an OD of 0.79 at 10 µg/mL (Figure 8D).

The antioxidant activity of Pd(II) complex is attributed to the combined effects of the Schiff base structure and the redox-active Pd center. Hydrogen atom transfer (HAT) and single electron transfer (SET) mechanisms would have been involved in the antioxidant capacity of Pd(II) complex [57]. The aromaticity of the indenoquinoxaline moiety and the presence of electron-donating nitrogen in the phenyl hydrazine unit would augment the Pd(II) complex's ability to participate in HAT and SET pathways. Thus, the synergistic interplay between the structural elements of the Schiff base and the redox-active Pd(II) Centre accounts for the potent antioxidant activity observed, with potential implications for therapeutic antioxidant applications [25, 58-61].

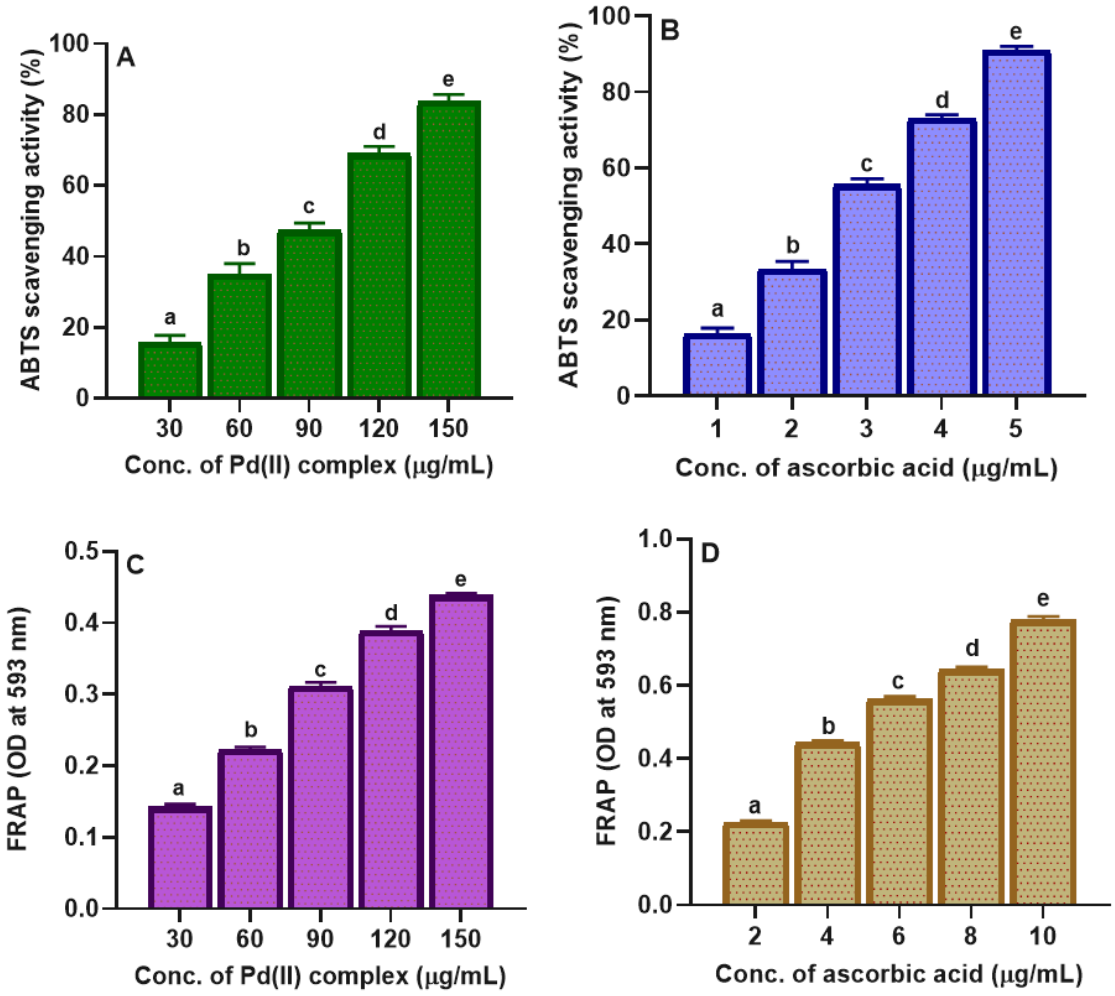

Figure 8. In vitro antioxidant activity. ABTS radical scavenging activity of Pd (II) complex **(A)** and standard ascorbic acid **(B).** FRAP activity of Pd (II) complex **(C)** and standard ascorbic acid **(D)**. Data are presented as mean ± SD, and significant differences ($P < 0.05$) between groups are indicated by different letters (a-e) in each assay

3.7 Antimicrobial Activity of Pd (II) Complex

The ZOI assay demonstrated a clear concentration-dependent increase in antimicrobial activity (Figure 9A-B). Statistical analysis using one-way ANOVA confirmed significant differences among treatment groups ($P < 0.05$), as indicated by distinct lettering in the graphical representation (Figure 9C). The MIC values further substantiated the inhibitory potential of the Pd (II) complex. The compound exhibited an MIC of 0.721 mg/mL against *S. aureus* and 0.635 mg/mL against *C. albicans*, indicating slightly higher sensitivity of the fungal strain (Figure 9D). MBC (Figure 6E–G) and MFC (Figure 9H–J) analyses revealed that the Pd (II) complex exerted bactericidal and fungicidal effects at concentrations above the MIC. Complete inhibition of microbial growth was observed upon subculturing at higher concentrations. The calculated MBC/MIC and MFC/MIC ratios were 1.39 for *S. aureus* and 1.57 for *C. albicans*, respectively. Since these values are less than 4, the Pd (II) complex can be classified as bactericidal against *S. aureus* and fungicidal against *C. albicans* rather than merely inhibiting microbial growth. Previous studies have shown that indenoquinoxaline derivatives or hybrid molecules as well as Pd-Schiff base complexes exhibited antimicrobial activity [28, 62-65]. Several plausible pathways have been proposed for these compounds antimicrobial activity which includes microbial cell wall disruption, ROS generation, and DNA interaction [66-68]. Additionally, Pd(II) complexes have been reported to inhibit the N or A efflux pump, thereby resensitizing fluoroquinolone-resistant *S. aureus* strains [69]. In line with previous reports, the synthesized Pd–Schiff base complex demonstrated notable antimicrobial activity in the present study; however, the exact molecular mechanism underlying this bioactivity remains to be elucidated to support its potential clinical application.

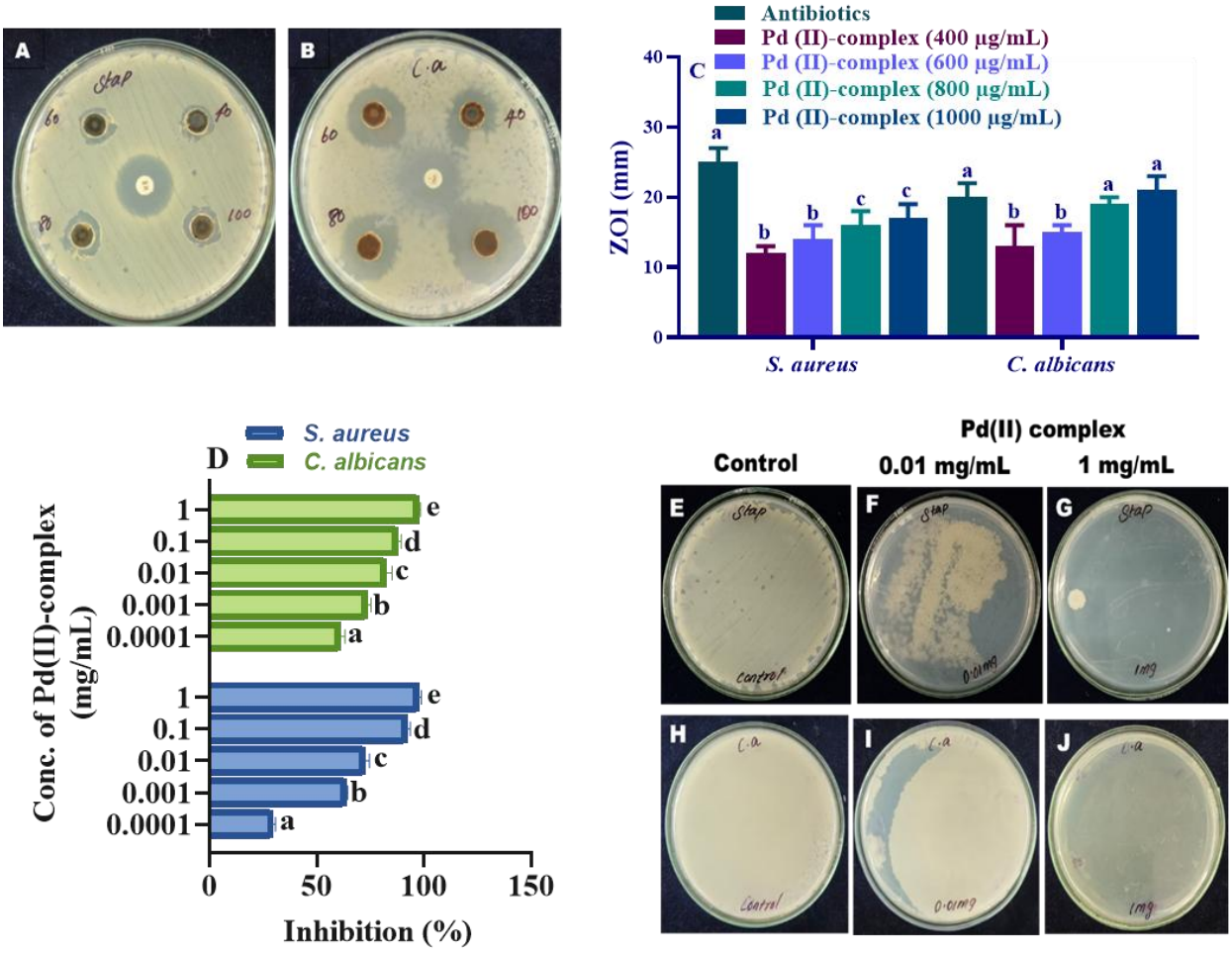

Figure 9. Representative images showing ZOI by Pd (II) complex against **(A)** *S. aureus* and **(B)** *C. albicans*. **(C)** ZOI comparison showing concentration-dependent antimicrobial potency. **(H)** MIC curve for *S. aureus* and *C. albicans* demonstrating progressive inhibition with increasing Pd (II) concentration **(D). (E-G)** Representative images showing MBC against *S. aureus*. **(H-J)** Representative images showing MBC against *C. albicans*. Different letters (a–e) denote statistically significant differences ($P < 0.05$).

3.8 A-Amylase Inhibition by Pd (II) Complex

The Pd (II) complex exhibited a clear, concentration-dependent inhibition of α-amylase activity. At 100 µg/mL, the inhibition was modest (19.3 ± 3.5%), but it increased progressively with concentration, reaching 76.7 ± 2.5% at 500 µg/mL (Figure 10A). The IC_{50} value for the complex was determined to be 326.47 µg/mL, which, although significantly higher than that of the standard inhibitor acarbose (IC_{50} = 12.5 µg/mL), still indicates notable inhibitory activity (Figure 10B). Kinetic analysis revealed that the complex follows a mixed mode of inhibition, with a calculated Ki value of 302.56 µg/mL (Figure 10C and 10D).

3.9 In Silico Analysis: Binding of Pd (II) Complex with A-Amylase Details of Pd (II) Complex Interaction with Amino Acids Present In A-Amylase

The binding energy of the Pd (II) complex with the α-amylase enzyme was found to be -7.65 kcal/mol. The intermolecular interactions between the Pd (II) complex and the α-amylase enzyme during molecular docking and MD simulation are shown in Figure 9 Table 1 summarises the key interactions between the Pd (II) complex and α-amylase obtained from docking and MD simulations. Hydrogen bonding, hydrophobic, and electrostatic interactions were analysed to evaluate ligand binding stability and molecular recognition. The superimposed structure of the Pd (II) complex and α-amylase from docking and MD is shown in Figure 9A. The Pd (II) complex was oriented in the same site at the end of 100 ns MD, similar to that of docking indicating the stable binding of Pd (II) complex with α-amylase. In the docking analysis, hydrogen bonds were observed with Tyr151, Thr163, Asp197, His201, Glu233, Ile235, and Asp300, with bond distances ranging from 2.2 to 3.5 Å. Hydrophobic interactions involved Leu162, Ile235, Ala198, Lys200, and His201, with distances up to 4.8 Å. Electrostatic interactions were primarily mediated by His201 and Glu233, with interaction distances of 3.4 and 4.4 Å, respectively (Figure 11B and Table 1).

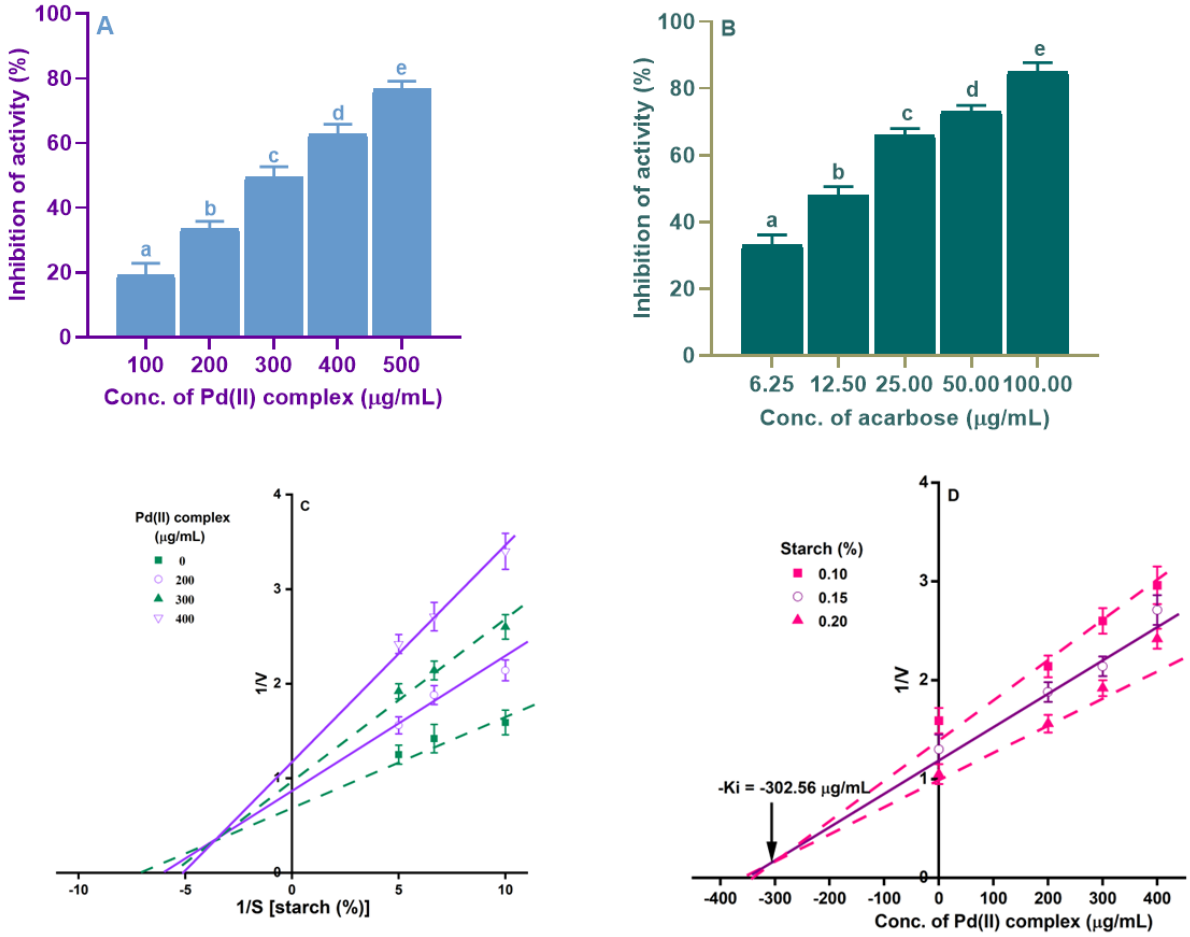

Figure 10. Enzyme inhibition. Dose-dependent inhibition of α-amylase by Pd-Schiff base ligand complex **(A)** and standard acarbose **(B)**. LB **(C)** and Dixon plot Pd-Schiff base ligand inhibition of α-amylase **(D)**. Data are presented as mean ± SD, and significant differences ($P < 0.05$) between groups are indicated by different letters (a-e) in each assay.

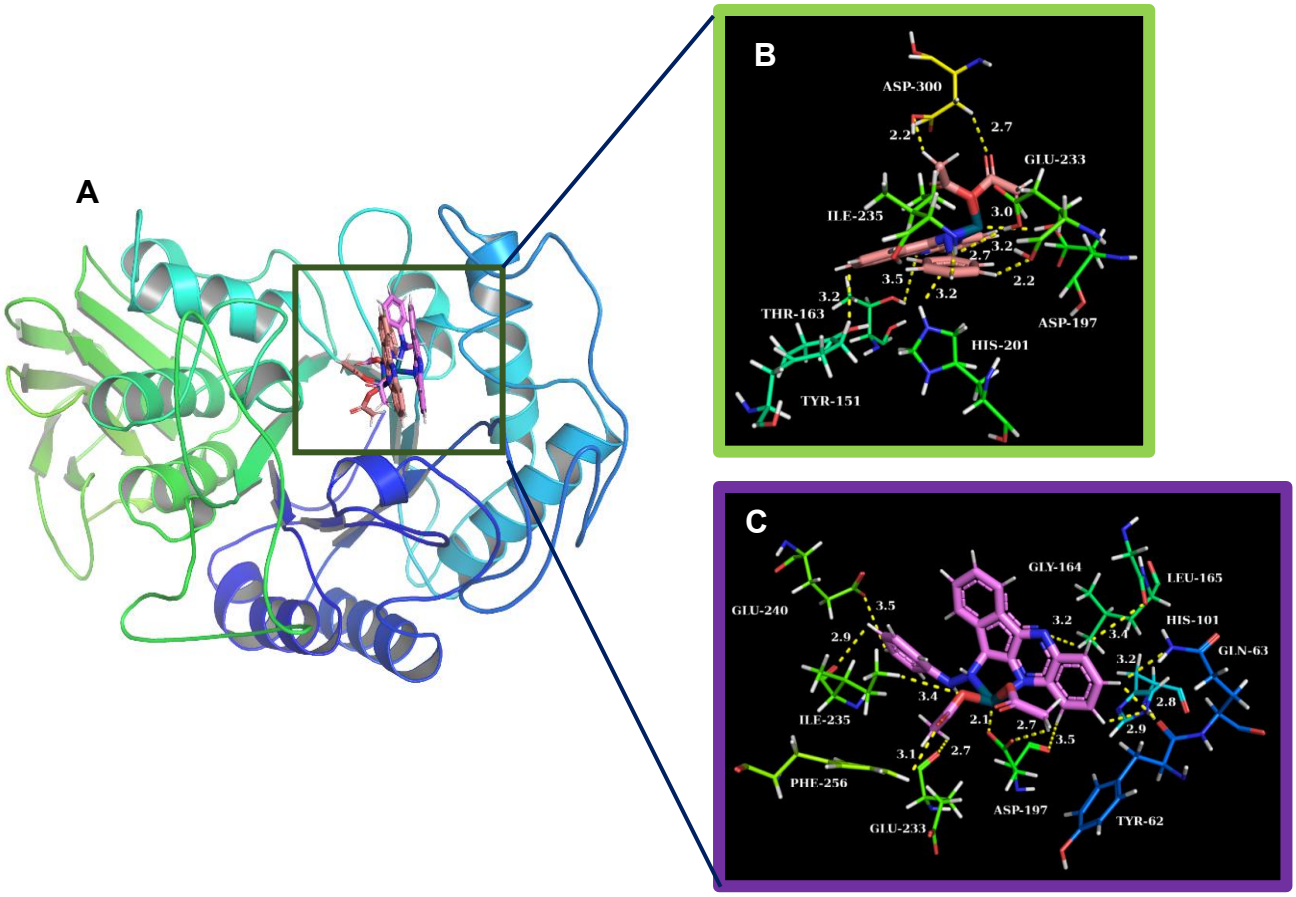

Figure 11. *In silico* analysis. **(A)** Superimposed structure of human α-amylase and Pd-Schiff base ligand during docking and at the end of 100 ns MD simulation. **(B)** Details of hydrogen bond interaction of Pd-Schiff base ligand with the amino acids present in human α-amylase during docking **(B)** and MD simulation **(C)**

Table 1. Intermolecular interactions of the Pd (II) complex with α-amylase (distance in Å)

Pd(II) complex/α-amylase	Hydrogen bonding interactions	Hydrophobic interactions	Electrostatic interactions
Docking	Tyr151 (3.2), Thr163 (3.5), Asp197 (3.0), His201 (3.2), Glu233 (2.7), Ile235 (3.2), Asp300 (2.2)	Leu162 (3.3), Ile235 (3.6), Ala198 (4.8), Lys200 (4.8), His201 (4.2)	His201 (3.4), Glu233 (4.4)
MD	Tyr62 (2.8), Gln63 (3.2), His101 (2.9), Gly164 (3.2), Leu165 (3.4), Asp197 (2.7), Glu233 (2.7), Ile235 (2.9), Glu240 (3.5), Phe256 (3.1)	Leu162 (5.0), Leu165 (4.6), Ala198 (4.6), Ile235 (4.5)	Asp197 (2.1)

MD simulations revealed a shift in key interacting residues, suggesting ligand–Pd complex-induced conformational changes in α-amylase. Hydrogen bonding interactions were formed with Tyr62, Gln63, His101, Gly164, Leu165, Asp197, Glu233, Ile235, Glu240, and Phe256, with bond distances ranging from 2.7 to 3.5 Å. Hydrophobic interactions involved Leu162, Leu165, Ala198, and Ile235, with interaction distances between 4.5 and 5.0 Å. Electrostatic interactions were reduced, with Asp197 being the primary contributor (2.1 Å) (Figure 11 C and Table 1).

3.10 RMSD and RMSF Analysis

The RMSD and RMSF plots of ligand–Pd complex/α-amylase enzyme complex are shown in Figure 9A and 9B, respectively. The RMSD plot confirms no large conformational modifications during the MD simulation. The RMSD value of the ligand–Pd complex molecule possesses a high stability nature. From starting to 20 ns time, the ligand molecule shows the range of 1 to 1.4 Å, and after that, the molecule remains stable in the range of 1.7 Å. The RMSD value of α-amylase enzyme is also within 2.5 Å, up to 100 ns MD

simulation. The RMSF plots indicate the high fluctuations of the loop region around the active site of the enzyme due to ligand–Pd complex binding conformational modifications. However, the value is low for all the amino acids except the terminal region. In particular, α-helix to loop conformational modifications happened for the region Trp58-Tyr62 from molecular docking to MD simulation. The relative RMSF values of those amino acids are about 3-4 Å. The residues Asn137-Gly139 undergo loop to α-helix conformational modifications, with the RMSF values around 4 Å (Figure 12 and Table 2).

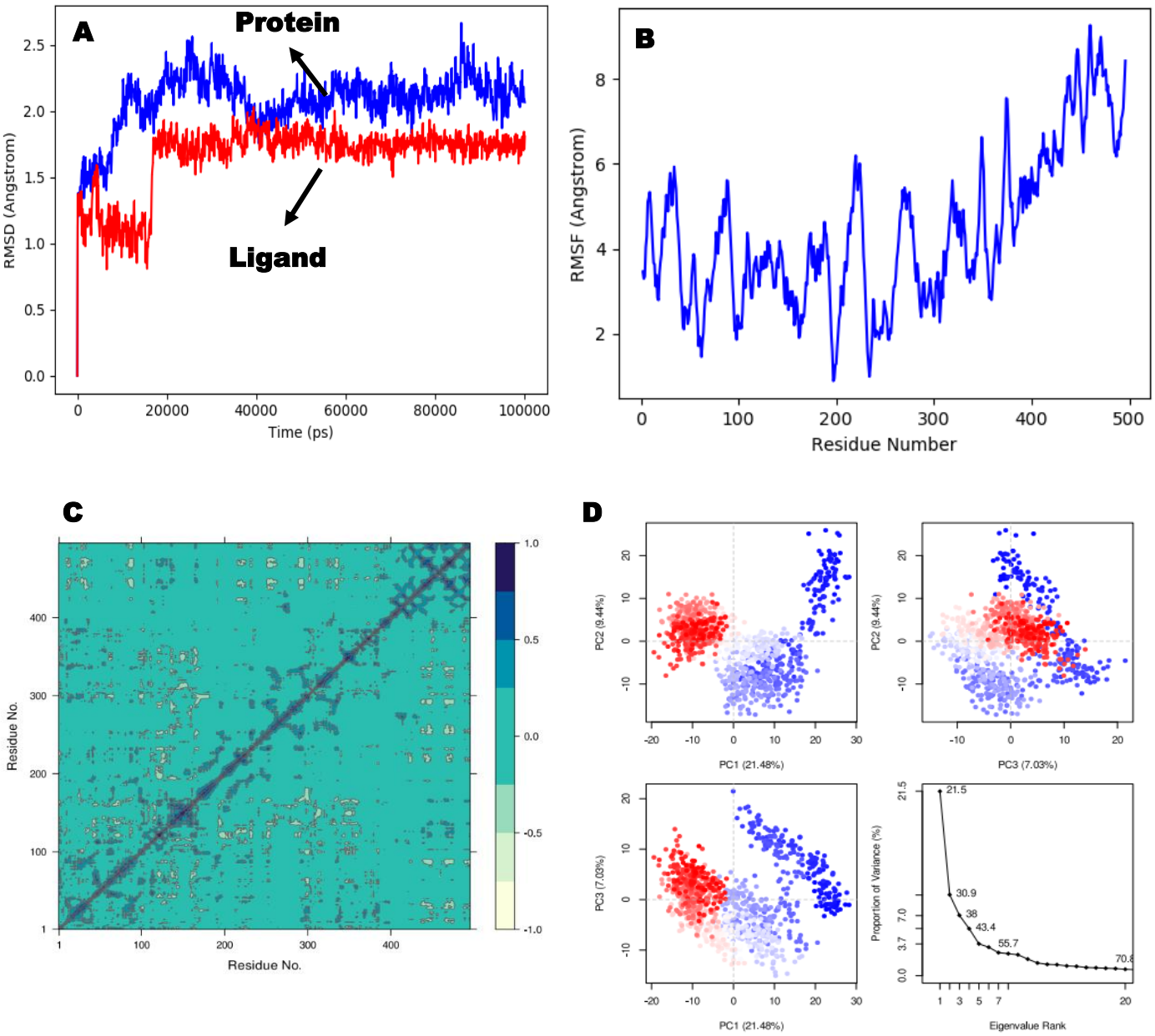

Figure 12. (A) RMSD, (B) RMSF, (C) DCCM, and (D) PCA of Pd-Schiff base ligand complex/α-amylase complex throughout 100 ns MD simulation.

Table 2. MM/GBSA binding free energy of Pd (II) complex with α-amylase

ΔG Bind	Coulomb	Covalent	H bond	Lipo	vdW
kcal/mol					
-61.4	8.5	7.7	-1.4	-29.1	-43.4

3.11 PCA and DCCM Analysis

Figure 9C presents the DCCM derived from MD simulations of the ligand–Pd complex/enzyme complex. The correlation coefficients, ranging from -1.0 (light yellow) to 1.0 (dark blue), provide insights into the extent of concerted motion between residue pairs. Positive correlation values indicate residues moving in a concerted manner, while negative correlation (anti-correlation) values signify residues moving in opposing directions. The strong positive correlations along the diagonal indicate expected sequential residue interactions due to local secondary structural elements, such as α-helices and β-strands. Beyond the diagonal, distinct regions exhibit significant positive correlation, particularly in residues spanning positions 56–126 and 306–386, suggesting long-range cooperative motions. These interactions likely reflect structural coupling between functional domains, which may be essential for maintaining enzymatic activity.

Additionally, clusters of strong anti-correlation are observed between residues 86–156 and 256–406, indicating dynamic fluctuations that may facilitate conformational changes required for substrate binding or product release. The presence of these correlated and anti-correlated regions highlights the role of ligand binding in modulating the enzyme's internal dynamics. Specifically, the ligand-induced stabilization of certain residue pairs appears to enhance structural rigidity in the active site region while promoting flexibility in distal regions, potentially enabling allosteric regulation.

The observed long-range correlations suggest that ligand binding influences global protein motions, which could be crucial for catalytic efficiency and specificity. The correlation distribution suggests a heterogeneous dynamic landscape, with distinct clusters of residues exhibiting strong cooperative motion while other regions remain relatively independent. This phenomenon indicates the tight binding of the ligand–Pd complex with the active site residues, while other amino acids support the relative binding. These findings underscore the importance of dynamic coupling between structurally distant residues in enzyme function. PCA was applied to identify the key dynamic features of the complexes. Figure 9D presents the results of the PCA performed on the MD simulation trajectory of the ligand-enzyme complex. The scatter plots of the first three principal components (PC1, PC2, and PC3) illustrate the conformational clustering of the system. PC1 accounts for 21.48% of the total variance, followed by PC2 with 9.44% and PC3 with 7.03%, indicating that a significant portion of the system's motions can be captured by these three components.

Distinct clustering of conformations is observed in the PC space, where red and blue colour gradients indicate different conformational states sampled during the simulation. The separation along PC1 suggests a dominant global motion, likely corresponding to large-scale domain rearrangements or hinge-like motions. The spread along PC2 and PC3 indicates additional conformational flexibility, which may contribute to functional transitions between different enzyme states. The scree plot (bottom right panel) further supports these observations, with a sharp decline in variance after the first few principal components, suggesting that the majority of relevant dynamical information is concentrated in the leading PCs. These results indicate that the ligand binding event induces distinct conformational sub-states, which may be crucial for catalytic activity and allosteric regulation. Further analysis of the eigenvectors associated with PC1 and PC2 could provide deeper insights into the specific residue movements contributing to these dominant motions.

3.12 MM/GBSA Free Energy Calculations

The MM/GBSA calculations provided insights into the binding free energy components for the ligand-α-amylase complex. The total binding free energy (ΔG Bind) was calculated to be -61.4 kcal/mol, indicating a strong binding affinity between the ligand and α-amylase. Among the contributing energy terms, van der Waals interactions (ΔvdW) were the most significant, contributing -43.4 kcal/mol, followed by lipophilic interactions (ΔLipo) at -29.1 kcal/mol. These findings highlight the dominant role of hydrophobic interactions in stabilising the ligand-enzyme complex.

Electrostatic interactions, represented by Coulomb energy, contributed 8.5 kcal/mol, suggesting that while electrostatic forces play a role, they are not the primary driving factor in ligand binding. Covalent interactions also contributed positively (7.7 kcal/mol), indicating some degree of covalent stabilisation. Hydrogen bonding (ΔH bond) exhibited a minor unfavourable contribution of -1.4 kcal/mol, suggesting that specific hydrogen bonds may not be a major factor in the overall binding affinity. These results indicate that the ligand binding is primarily driven by van der Waals and lipophilic interactions, with minor contributions from electrostatics and hydrogen bonding interactions.

Diabetes is a growing global health concern, with projections indicating a significant rise in cases by 2045 (70). Enzymes like α-amylase and α-glucosidase play a central role in carbohydrate digestion and postprandial hyperglycemia. While current enzyme inhibitors like acarbose are effective, they often cause gastrointestinal side effects. Consequently, there is increasing interest in developing synthetic inhibitors with improved efficacy and tolerability (8, 25). Previous studies have reported the α-amylase inhibitory effect of Schiff bases (thiadiazol-based Schiff bases, thiazole-based Schiff bases, benzimidazole-based Schiff bases, and indazole-based Schiff bases) and indenoquinoxaline derivatives (25, 27, 71-73). Pd(II) complexes have also been reported for their ability to

suppress the activity of α-amylase and α-glucosidase (74). In another study, newly synthesized 4-hydroxy Pd-C-III derivatives demonstrated dual inhibitory action by targeting both α-glucosidase and protein tyrosine phosphatase 1B (PTP1B), indicating their promise in modulating glucose metabolism and insulin signaling pathways (75). Similar to these reports, the newly synthesized Pd(II) complex has inhibited the α-amylase. The kinetic analysis indicating a mixed mode of inhibition, suggests that the Pd-Schiff base complex interacts with both the free enzyme and the enzyme–substrate complex, potentially enhancing its inhibitory efficacy through multiple binding interactions. The *in vitro* result was corroborated by *in silico* molecular docking and MD analysis. Pd-Schiff base complex was found to bind in the active site of α-amylase (44). The comparison between docking and MD results highlighted the dynamic nature of ligand binding and its strong binding within the active site. The ligand showed orientation in the active site, forming stable binding with the catalytic site amino acids Asp197 (catalytic nucleophile) and Glu233 (catalytic proton donor) (44). Persistent hyperglycaemia and oxidative stress are key drivers of diabetic complications, while elevated glucose levels and immune dysfunction increase susceptibility to microbial infections in diabetic individuals (76,77). Given this, the multifunctional nature of the synthesized Pd-Schiff base complex, demonstrating antioxidant, antimicrobial, and α-amylase inhibitory activities, positions it as a compelling lead for the development of therapeutic agents targeting both diabetes and its associated secondary complications.

4. Conclusions

A new quinoxaline Schiff base ligand and its Pd (II) complex were synthesized and characterized in good yield. The present study highlights the potential of the newly synthesized Pd (II) complex as a promising multifunctional therapeutic agent. Its demonstrated antioxidant capacity, effective inhibition of α-amylase through a mixed mode of action, and significant antimicrobial activity underscore its relevance in addressing hyperglycaemia and managing secondary complications associated with diabetes. In silico molecular docking analysis further supported these findings, revealing strong binding affinity of the complex to the active site of human α-amylase, with interactions involving key catalytic residues. These combined experimental and computational results support further investigation into the complex's mechanism of action and in vivo efficacy, paving the way for its development in antidiabetic drug discovery and the management of related complications.

References

[1] M.A. Mir, B.K. Banik, Synthesis of Schiff Base Ligands Under Environment Friendly Conditions: A Systematic Review. Inorganic Chemistry Communications, 174(part 1), (2025) 113987. https://doi.org/10.1016/j.inoche.2025.113987

[2] P.E. Marinova, K.D. Tamahkyarova, Synthesis, Investigation, Biological Evaluation, and Application of Coordination Compounds with Schiff Base—A Review, Compounds, 5(2), (2025) 14. https://doi.org/10.3390/compounds5020014

[3] S. Bano, F. Arshi, S. Firdaus, N.K. Kushwaha, S.K. Singh, A. Kumar, A.K. Singh, Exploring Schiff base and its Palladium Complexes: Synthesis, Characterization, Antimycobacterial Activity, DFT, Molecular Docking and ADME Studies. Journal of Molecular Structure, (2025) 143704. https://doi.org/10.1016/j.molstruc.2025.143704

[4] D. Pantic, N. Mirkovic, T. Vulovic, D. Jovanovic, S. Jakovljevic, P. Canovic, M. Zaric, R.Z. Zaric, M. Kostic, J. Dragojevic, V. Divac, Evaluation of Newly Synthesized Schiff base Pd (II) Complexes for Prostate Cancer Treatment through in Vitro Cytotoxicity and Molecular Mechanistic Studies. Frontiers in Chemistry, *13*, (2025) 1636477. https://doi.org/10.3389/fchem.2025.1636477

[5] (a) S. Shanmugam, K. Radhakrishna, M. Jayakumar, P. Viswanathamurthi, and J.G. Malecki, Copper (I) Hydrazonate Complexes as Efficient Catalysts for Synthesizing Substituted Pyrimidines Via Acceptorless Dehydrogenative Coupling of Amidine and Alcohols. Inorganica Chimica Acta, 583, (2025) 122678. https://doi.org/10.1016/j.ica.2025.122678

[6] (b)S. Shanmugam, S. Gayathri, P. Viswanathamurthi, P. Vijayan, and J.G. Malecki, Efficient Synthesis of Highly Substituted Imidazoles Catalysed by Cu (I) Complexes Containing Phosphine Functionalised Hydrazone Ligands. *Applied Organometallic Chemistry*, 39, (2025) 70436. https://doi.org/10.1002/aoc.70436

[7] K.S. Mani, W. Kaminsky, S.P. Rajendran, A Facile Atom Economic One Pot Multicomponent Synthesis of Bioactive Spiro-Indenoquinoxaline Pyrrolizines as Potent Antioxidants and Anti-Cancer Agents. New Journal of Chemistry, 42(1), (2018) 301–310. https://doi.org/10.1039/C7NJ02993D

[8] S. Sawant, P. Patil, G. Salunke, R. Kamble, M. Bharmal, S. Sankpal, K. Sonawane, S.

Hangirgekar, An Efficient, Catalyst-Free Synthesis of Novel Indenoquinoxaline Fused Hydrazinylthiazoles and their Antimicrobial Evaluation with Molecular Docking Study. Journal of Molecular Structure, 1321(part 5), (2025) 140069. https://doi.org/10.1016/j.molstruc.2024.140069

[9] S. Hameed, F. Saleem, M. Ozil, N. Baltaş, U. Salar, S. Ashraf, Z. Ul-Haq, M. Taha, K.M. Khan, Indenoquinoxaline-Phenylacrylohydrazide Hybrids as Promising Drug Candidates for the Treatment of Type 2 Diabetes: In Vitro and in Silico Evaluation of Enzyme Inhibition and Antioxidant Activity. International Journal of Biological Macromolecules, 263(part 2), (2024) 129517. https://doi.org/10.1016/j.ijbiomac.2024.129517

[10] L. Kavoosi, B. Aghamiri, F.M. Moghaddam, Regio- and Diastereoselective Synthesis of Indeno-Quinoxaline-Thiazolidine-2-Thione and bis-indeno-quinoxaline-dicarbamodithioate derivatives with Photoluminescent Properties and Potential Applications. Tetrahedron, 183, (2025) 134708. https://doi.org/10.1016/j.tet.2025.134708

[11] I.B. Obot, N.O. Obi-Egbedi, Indeno-1-One [2,3-B] Quinoxaline as an Effective Inhibitor for the Corrosion of Mild Steel in 0.5 M H_2SO_4 Solution. Materials Chemistry and Physics, 122(2–3), (2010) 325–328. https://doi.org/10.1016/j.matchemphys.2010.03.037

[12] C.W. Kayogolo, M.R. Vegi, B.B.L. Srivastava, M.G. Sahini, Therapeutical Potential of Metal Complexes of Quinoxaline Derivatives: A Review. Journal of Coordination Chemistry, 75(1–2), (2022) 1–48. https://doi.org/10.1080/00958972.2022.2049767

[13] M.P. Dhaduk, R.A. Dabhi, V.D. Bhatt, B.S. Bhatt, M.N. Patel, Synthesis, Characterization, Biomolecular Interaction, Cytotoxicity, and Computational Studies of Quinoxaline-based Platinum (II) Complexes. Results in Chemistry, 7, (2024) 101265. https://doi.org/10.1016/j.rechem.2023.101265

[14] K.J. Babu, D. Ayodhya, Shivaraj, Comprehensive Investigation of Co (II), Ni (II), and Cu(II) Complexes Derived from a Schiff Base: Synthesis, Characterization, DNA Interactions, ADME Profiling, Molecular Docking, and in-Vitro Biological Evaluation. Results in Chemistry, 6, (2023) 101110. https://doi.org/10.1016/j.rechem.2023.101110

[15] R.A.C. Souza, W.R.P. Costa, E.d.F. Faria, M.A.d.S. Bessa, R.d. Menezes, C.H.G. Martins, P.I.S. Maia, V.M. Deflon, C.G. Oliveira, Copper (II) Complexes based on Thiosemicarbazone Ligand: Preparation, Crystal Structure, Hirshfeld Surface, Energy Framework, Antimycobacterium Activity, *in Silico* and Molecular Docking Studies. Journal of Inorganic Biochemistry, 223, (2021) 111543. https://doi.org/10.1016/j.jinorgbio.2021.111543

[16] A. Mandal, A.T. Khan, Recent Advancement in the Synthesis of Quinoline Derivatives Via Multicomponent Reactions. Organic & Biomolecular Chemistry, 12, (2024). https://doi.org/10.1039/D4OB00034J

[17] J.G. Hernandez, I.S. Butler, T. Friscic, Multi-Step and Multi-Component Organometallic Synthesis in One Pot Using Orthogonal Mechanochemical Reactions. Chemical Science, 5(9), (2014) 3576–3582. https://doi.org/10.1039/C4SC01252F

[18] W. Ruankham, N. Songtawee, V. Prachayasittikul, A. Worachartcheewan, W. Suwanjang, R. Pingaew, V. Prachayasittikul, S. Prachayasittikul, K. Phopin, Promising 8-Aminoquinoline-Based Metal Complexes in Modulation of SIRT1/3-FOXO3a Axis against Oxidative Damage-Induced Preclinical Neurons. ACS Omega, 8(49), (2023) 46977–46988. https://doi.org/10.1021/acsomega.3c06764

[19] A.M. Waseem, R.M. Elmagzoub, M.M.M. Abdelgadir, A. Al Bahir, N.S. Abd El-Gawaad, A.S. Abdel-Samea, D.P. Rao, K. Kossenas, S. Brase, H. Hashem, Therapeutic Impact of Quinoxaline Derivatives: Recent Advances in Biological Activities. Results in Chemistry, 13, (2024) 101989. https://doi.org/10.1016/j.rechem.2024.101989

[20] W.A. Wani, A. Hussain, S. Amir, M.F. Alajmi, A.H. Malik, A. Khursheed, W.A. Khanday, Emergence of Macrocyclic Metal Complexes as Anticancer Agents. ACS Symposium Series, ACS Publications, 1492 (2025) 1–12. https://doi.org/10.1021/bk-2025-1492.ch001

[21] G.A. Eldeken, F.A. El-Samahy, E.M. Zayed, F.H. Osman, G.E.H. Elgemeie, Synthesis, Biological Activities and Molecular Docking analysis of a Novel Series of 11*H*-Indeno[1,2-*b*]quinoxalin-11-one Derivatives. Journal of Molecular Structure, 1261, (2022) 132929. https://doi.org/10.1016/j.molstruc.2022.132929

[22] A.B. Canaj, L.E. Nodaraki, K. Slepokura, M. Siczek, D.I. Tzimopoulos, T. Lis, C.J. Milios, A family of Polynuclear Cobalt Complexes Upon

Employment of an Indeno-Quinoxaline Based Oxime Ligand. RSC Advances, 4(44), (2014) 23068–23077. https://doi.org/10.1039/C4RA01914H

[23] C.J. Dhanaraj, J. Johnson. Metal Complexes of Quinoxaline Derivatives: Review (part 1). Research Journal of Chemical Sciences, 4(11) (2014) 80-102.

[24] S. Sarkar, S. Biswas, K. Dey, Synthesis, spectroscopic Characterization and Magnetic Properties of Homo- and Heterodinuclear Complexes of Transition and Non-Transition Metal Ions with a New Schiff Base Ligand. Spectrochimica Acta Part A: Molecular and Biomolecular Spectroscopy, 17(4), (2008), 1555-1561. https://doi.org/10.1016/j.saa.2008.06.002

[25] I. Tsacheva, Z. Todorova, D. Momekova, G. Momekov, N. Koseva, Pharmacological Activities of Schiff Bases and their Derivatives with Low and High Molecular Phosphonates. Pharmaceuticals, 16(7), (2023) 938. https://doi.org/10.3390/ph16070938

[26] S. Hameed, K.M. Khan, U. Salar, M. Ozil, N. Baltaş, F. Saleem, U. Qureshi, M. Taha, Z. Ul-Haq, Hydrazinyl Thiazole Linked Indenoquinoxaline Hybrids: Potential Leads to Treat Hyperglycemia and Oxidative Stress; Multistep Synthesis, A-Amylase, A-Glucosidase Inhibitory and Antioxidant Activities. International Journal of Biological Macromolecules, 221, (2022) 1294–1312. https://doi.org/10.1016/j.ijbiomac.2022.09.102

[27] A.M. Abdallah, S.M. Gomha, M.E.A. Zaki, T.Z. Abolibda, N.A. Kheder, A Green Synthesis, DFT Calculations, and Molecular Docking Study of Some New Indeno[2,1-*B*] Quinoxalines Containing Thiazole Moiety. Journal of Molecular Structure, 1292, (2023) 136044. https://doi.org/10.1016/j.molstruc.2023.136044

[28] N.A. Gohar, E.A. Fayed, Y.A. Ammar, O.A. Abu Ali, A. Ragab, A.M. Mahfoz, M.S. Abusaif, Fluorinated Indeno-Quinoxaline Bearing Thiazole Moieties as Hypoglycaemic Agents Targeting *A*-Amylase, and *A*-Glucosidase: Synthesis, Molecular Docking, and ADMET Studies. Journal of Enzyme Inhibition and Medicinal Chemistry, 39(1), (2024) 2367128. https://doi.org/10.1080/14756366.2024.2367128

[29] N. Bouali, M.B. Hammouda, I. Ahmad, S. Ghannay, A. Thouri, A. Dbeibia, H. Patel, W.S. Hamadou, K. Hosni, M. Snoussi, M. Adnan, M.I. Hassan, E. Noumi, K. Aouadi, A. Kadri, Multifunctional Derivatives of Spiropyrrolidine Tethered Indeno-Quinoxaline Heterocyclic Hybrids as Potent Antimicrobial, Antioxidant and Antidiabetic Agents: Design, Synthesis, In Vitro and In Silico Approaches. Molecules, 27(21), (2022) 7248. https://doi.org/10.3390/molecules27217248

[30] H. Abebe, T. Lamma, A. Filkale, D. Kure, (2024). Synthesis, Charactrization and Antibacterial Activity of Schiff Bases Derived from Phenyl Hydrazine Derivatives and their Cu (II) and Zn (II) Complexes. https://doi.org/10.26434/chemrxiv-2024-d4cjt

[31] P.E. Marinova, K.D. Tamahkyarova. Synthesis, Investigation, Biological Evaluation and Application of Coordination Compounds-A Review. 5(2), (2024). https://www.preprints.org/manuscript/202412.0830

[32] V.K. Juyal, A. Pathak, M. Panwar, S.C. Thakuri, O. Prakash, A. Agrwal, V. Nand, Schiff base Metal Complexes as Versatile Catalysts: A Review. Journal of Organometallic Chemistry, 999, (2023) 122825. https://doi.org/10.1016/j.jorganchem.2023.122825

[33] H. Kargar, M. Fallah-Mehrjardi, R. Behjatmanesh-Ardakani, M. Bahadori, M. Moghadam, M. Ashfaq, K.S. Munawar, M.N. Tahir, Spectroscopic Investigation, Molecular Structure, Catalytic Activity with Computational Studies of a Novel Pd(II) Complex Incorporating Unsymmetrical Tetradentate Schiff Base Ligand. Inorganic Chemistry Communications, 142, (2022) 109697. https://doi.org/10.1016/j.inoche.2022.109697

[34] S. Celedon, T. Roisnel, V. Artigas, M. Fuentealba, D. Carrillo, I. Ledoux-Rak, J.-R. Hamon, C. Manzur, Palladium(ii) Complexes of Tetradentate Donor–Acceptor Schiff Base Ligands: Synthesis and Spectral, Structural, Thermal and NLO Properties. New Journal of Chemistry, 44(22), (2020) 9190–9201. https://doi.org/10.1039/D0NJ01982H

[35] C. Boulechfar, H. Ferkous, A. Delimi, A. Djedouani, A. Kahlouche, A. Boublia, A.S. Darwish, T. Lemaoui, R. Verma, Y. Benguerba, Schiff bases and their metal Complexes: A Review on the History, Synthesis, and Applications. Inorganic Chemistry Communications, 150, (2023) 110451. https://doi.org/10.1016/j.inoche.2023.110451

[36] M. Al-Azzawi, İ. Yılmaz, H.E. Bostancı, Synthesis and Anti-Cancer Properties of Pd(II) and Pt(II) Coordination Compounds of

Heterocyclic Schiff base Ligands. Journal of Molecular Structure, 1337, (2025) 142199. https://doi.org/10.1016/j.molstruc.2025.142199

[37] R. Sankar, T.M. Sharmila, Schiff bases-based Metallo Complexes and their Crucial Role in the Realm of Pharmacology. A review. Results in Chemistry, 6, (2023) 101179. https://doi.org/10.1016/j.rechem.2023.101179

[38] A. Soroceanu, A. Bargan, Advanced and Biomedical Applications of Schiff-Base Ligands and Their Metal Complexes: A Review. Crystals, 12(10), (2022) 1436. https://doi.org/10.3390/cryst12101436

[39] N. Turan, K. Buldurun, E. Bursal, G. Mahmoudi, Pd (II)-Schiff base complexes: Synthesis, Characterization, Suzuki–Miyaura and Mizoroki–Heck Cross-Coupling Reactions, Enzyme Inhibition and Antioxidant Activities. Journal of Organometallic Chemistry, 970-971, (2022) 122370. https://doi.org/10.1016/j.jorganchem.2022.122370

[40] R. Vallavoju, R. Kore, R. Parikirala, M. Subburu, R. Gade, V. Kumar, M. Raghavender, P. Chetti, S. Pola, Synthesis and Characterization of New Tetradentate N_2O_2-Based Schiff's Base Cu (II) Complexes for Dye Photodegradation. Photochem, 3(2), (2023) 274–287. https://doi.org/10.3390/photochem3020016

[41] I.H. Hasan, R.M. Mhaibes, A.A.H. Kadhum, H.A. Al-Bahrani, A.T.A. Imeer, N.A.M. Al-Rashedi, G. Shu, Recent Advances on Pd schiff base Catalysts in Suzuki-Miyaura Cross-Coupling Reaction: A Review. Journal of Organometallic Chemistry, 1024, (2024) 123444. https://doi.org/10.1016/j.jorganchem.2024.123444

[42] R. Re, N. Pellegrini, A. Proteggente, A. Pannala, M. Yang, C. Rice-Evans, Antioxidant Activity Applying an improved ABTS Radical Cation Decolorization Assay. Free Radical Biology and Medicine, 26(9–10), (1999) 1231–1237. https://doi.org/10.1016/S0891-5849(98)00315-3

[43] I.F.F. Benzie, J.J. Strain, The Ferric Reducing Ability of Plasma (FRAP) as a Measure of Antioxidant Power: The FRAP Assay. Analytical Biochemistry, 239(1), (1996) 70–76. https://doi.org/10.1006/abio.1996.0292

[44] A.P. Mohideen, C. Loganathan, M.S. Khan, M.H. Abdelzaher, N. Alsanousi, S.B. Dayel, Green Synthesis and Characterization of Zinc Oxide Nanoparticles Mediated by Nyctanthes arbor-tristis Leaf Extract: Exploring Antidiabetic, Anticancer, and Antimicrobial Activities. Journal of Cluster Science, 36(2), (2025) 57. https://doi.org/10.1007/s10876-025-02778-2

[45] L.K. Williams, C. Li, S.G. Withers, G.D. Brayer, Order and Disorder: Differential Structural Impacts of Myricetin and Ethyl Caffeate on Human Amylase, an Antidiabetic Target. Journal of Medicinal Chemistry, 55(22), (2012) 10177–10186. https://doi.org/10.1021/jm301273u

[46] G.M. Morris, R. Huey, W. Lindstrom, M.F. Sanner, R.K. Belew, D.S. Goodsell, A.J. Olson, AutoDock4 and AutoDockTools4: Automated Docking with Selective Receptor Flexibility. Journal of Computational Chemistry, 30(16), (2009) 2785–2791. https://doi.org/10.1002/jcc.21256

[47] S. Vijayan, C. Loganathan, P. Sakayanathan, P.J. Thayumanavan, In Silico and in Vitro Investigation of Anticancer Effect of Newly Synthesized Nonivamide-S-Allyl Cysteine Ester. Journal of Biomolecular Structure and Dynamics, 40(22), (2022) 11511–11525. https://doi.org/10.1080/07391102.2021.1959404

[48] K.J. Bowers, E. Chow, H. Xu, R.O. Dror, M.P. Eastwood, B.A. Gregersen, J.L. Klepeis, I. Kolossvary, M.A. Moraes, F.D. Sacerdoti, Scalable Algorithms for Molecular Dynamics Simulations on Commodity Clusters. Proceedings of the ACM/IEEE Conference on Supercomputing, (2006) 84-es. https://doi.org/10.1145/1188455.1188544

[49] P. Johnson, C. Loganathan, A. Iruthayaraj, K. Poomani, P.J. Thayumanavan, S-allyl cysteine as potent anti-gout drug: Insight into the Xanthine Oxidase Inhibition and Anti-Inflammatory Activity. Biochimie, 154, (2018) 1–9. https://doi.org/10.1016/j.biochi.2018.07.015

[50] P. Sakayanathan, C. Loganathan, S. Kandasamy, R.V. Ramanna, K. Poomani, P.J. Thayumanavan, In Vitro and in Silico Analysis of Novel Astaxanthin-S-Allyl Cysteine as an Inhibitor of Butyrylcholinesterase and Various Globular forms of Acetylcholinesterases. International Journal of Biological Macromolecules, 140, (2019) 1147–1157. https://doi.org/10.1016/j.ijbiomac.2019.08.168

[51] N. Ashraf, A. Asari, N. Yousaf, M. Ahmad, M. Ahmed, A. Faisal, M. Saleem, M.J. Muddassar, Combined 3D-QSAR, Molecular Docking and Dynamics Simulations Studies to Model and

Design TTK Inhibitors. Frontiers in Chemistry, 10, (2022) 1003816. https://doi.org/10.3389/fchem.2022.1003816

[52] D.R. Roe, T.E. Cheatham III, PTRAJ and CPPTRAJ: Software for Processing and Analysis of Molecular Dynamics Trajectory Data. Journal of Chemical Theory and Computation, 9(7), (2013) 3084–3095. https://doi.org/10.1021/ct400341p

[53] J. Li, R. Abel, K. Zhu, Y. Cao, S. Zhao, R.A. Friesner, The VSGB 2.0 model: A Next Generation Energy Model for High Resolution Protein Structure Modeling. Proteins: Structure, Function, and Bioinformatics, 79(10), (2011) 2794–2812. https://doi.org/10.1002/prot.23106

[54] E. Wang, H. Sun, J. Wang, Z. Wang, H. Liu, J.Z. Zhang, T. Hou, End-Point Binding Free Energy Calculation with MM/PBSA and MM/GBSA: Strategies and Applications in Drug Design. Chemical Reviews, 119(16), (2019) 9478–9508. https://doi.org/10.1021/acs.chemrev.9b00055

[55] S. Genheden, U. Ryde, The MM/PBSA and MM/GBSA Methods to Estimate Ligand-Binding Affinities. Expert Opinion on Drug Discovery, 10(5), (2015) 449–461. https://doi.org/10.1517/17460441.2015.1032936

[56] M.S. Rana, N.M.A. Rayhan, M.S.H. Emon, M.T. Islam, K. Rathry, M.M. Hasan, M.M.I. Mansur, B.C. Srijon, M.S. Islam, A. Ray, Antioxidant Activity of Schiff base Ligands using the DPPH Scavenging Assay: An Updated Review. RSC Advances, 14(45), (2024) 33094–33123. https://doi.org/10.1039/D4RA04375H

[57] M. Sedighipoor, A.H. Kianfar, G. Mohammadnezhad, H. Gorls, and W. Plass, Unsymmetrical Palladium (II) N, N, O, O-Schiff base Complexes: Efficient Catalysts for Suzuki Coupling Reaction. Inorganica Chimica Acta, 476, (2018) 20-26. https://doi.org/10.1016/j.ica.2018.02.007

[58] R.R. H, R.K. P, B. Das, Synthesis, Characterization and Antioxidant Activity of New β-Benzylselenated Schiff bases and their Palladium Complexes. Journal of Coordination Chemistry, 75(9–10), (2022) 1273–1288. https://doi.org/10.1080/00958972.2022.2106561

[59] I. Waziri, T.L. Yusuf, H.A. Zarma, S.O. Oselusi, L.C.C. Coetzee, A.S. Adeyinka, New Palladium (II) Complexes from Halogen Substituted Schiff base Ligands: Synthesis, Spectroscopic, Biological Activity, Density Functional Theory, and Molecular Docking Investigations. Inorganica Chimica Acta, 552, (2023) 121505. https://doi.org/10.1016/j.ica.2023.121505

[60] S. Thakur, A. Jaryal, A. Bhalla. Recent Advances in Biological and Medicinal Profile of schiff bases and their Metal Complexes: An updated version (2018–2023). Results in Chemistry, 7, (2024) 101350. https://doi.org/10.1016/j.rechem.2024.101350

[61] A. Husain, P. Ach, DNA Binding Affinities, Anti-Oxidant, Antimicrobial and Molecular Docking Activities of Pd (II) Complexes of Chromone Schiff bases. Journal of Molecular Structure, 1254, (2022) 132341. https://doi.org/10.1016/j.molstruc.2022.132341

[62] N. Arumugam, A.I. Almansour, R.S. Kumar, S.I. Alaqeel, V.S. Krishna, D. Sriram, Anti-Tubercular Activity of Novel Class of Spiropyrrolidine Tethered Indenoquinoxaline Heterocyclic Hybrids. Bioorganic Chemistry, 99, (2020) 103799. https://doi.org/10.1016/j.bioorg.2020.103799

[63] W. Ren, Q. Zhao, M. Yu, L. Guo, H. Chang, X. Jiang, Y. Luo, W. Huang, G. He, Design and Synthesis of Novel Spirooxindole–Indenoquinoxaline Derivatives as Novel Tryptophanyl-Trna Synthetase Inhibitors. Molecular Diversity, 24, (2020) 1043–1063. https://doi.org/10.1007/s11030-019-10011-2

[64] D. Iacopetta, J. Ceramella, A. Catalano, A. Mariconda, F. Giuzio, C. Saturnino, P. Longo, M.S. Sinicropi, Metal Complexes with Schiff bases as Antimicrobials and Catalysts. Inorganics, 11(8), (2023) 320. https://doi.org/10.3390/inorganics11080320

[65] B. Sharma, S. Shukla, R. Rattan, M. Fatima, M. Goel, M. Bhat, S. Dutta, R.K. Ranjan, M. Sharma, Antimicrobial Agents based on Metal Complexes: Present Situation and Future Prospects. International Journal of Biomaterials, 2022(1), (2022) 6819080. https://doi.org/10.1155/2022/6819080

[66] L. de Oliveira Amaral, L.R. Santiago, W.V. Ferreira, J.D.S. da Silva, A.J. Bortoluzzi, M.B. Marques, M.J.F. Costa, P.H. Sette-de-Souza, S.M. Soares, Novel Palladium(II) Complexes with Schiff bases Derived from 4,5-Methylenedioxy-2-Nitrobenzaldehyde And 5-Bromo-2-Hydroxybenzaldehyde as Potential Antimicrobial Agents: Synthesis, Characterization and Studies in Vitro. Journal of Molecular Structure, 1328, (2025) 141403. https://doi.org/10.1016/j.molstruc.2025.141403

[67] A. Kumar, S. Ahmed, M. Bhardwaj, S. Imtiaz, D. Kumar, A.R. Bhat, B. Sood, S. Maji, In Vitro Anti-Microbial, DNA-Binding, In

silico Pharmacokinetics and Molecular Docking Studies of Schiff-based Cu(II), Zn(II) and Pd(II) complexes. Journal of Molecular Structure, 1315, (2024) 138695. https://doi.org/10.1016/j.molstruc.2024.138695

[68] O.A. Zalevskaya, Y.A. Gur'eva, A.V. Kutchin, Palladium Complexes as Antimicrobial Agents. Russian Chemical Reviews, 92(9), (2023). https://rcr.colab.ws/publications/10.59761/RCR5093#

[69] R. Shobana, J.H. Thahirunnisa, S. Sivaprakash, A.J. Amali, A.P. Solomon, D. Suresh, Effect of Palladium(II) Complexes on NorA Efflux Pump Inhibition and Resensitization of Fluoroquinolone-Resistant Staphylococcus Aureus: in Vitro and in Silico Approach. Frontiers in Cellular and Infection Microbiology, 13, (2024) 1340135. https://doi.org/10.3389/fcimb.2023.1340135

[70] N.H. Cho, J.E. Shaw, S. Karuranga, Y. Huang, J.D. da Rocha Fernandes, A.W. Ohlrogge, B. Malanda, IDF Diabetes Atlas: Global Estimates of Diabetes Prevalence for 2017 and Projections for 2045. Diabetes Research and Clinical Practice, 138, (2018) 271–281.https://doi.org/10.1016/j.diabres.2018.02.023

[71] A. Shakoor, G. Fareed, I. Ahmad, A.A. Elhenawy, M. Khan, N. Fareed, E. Al-Olayan, M.R. Abukhadra, A. Alam, M. Ibrahim, Exploring the Anti-Diabetic Activity of Benzimidazole Containing Schiff Base Derivatives: In vitro α-amylase, α-glucosidase Inhibitions and in Silico Studies. Journal of Molecular Structure, 1321, (2025) 140136. https://doi.org/10.1016/j.molstruc.2024.140136

[72] M. Taha, S. Hayat, F. Rahim, N. Uddin, A. Wadood, M. Nawaz, M. Gollapalli, A.U. Rehman, K.M. Khan, R.K. Farooq, Exploring Thiazole-Based Schiff Base Analogs as Potent A-Glucosidase and A-Amylase Inhibitor: Their Synthesis and In-Silico Study. Journal of Molecular Structure, 1287, (2023) 135672. https://doi.org/10.1016/j.molstruc.2023.135672

[73] T. Zahoor, S. Khan, S. Chinnam, T. Iqbal, R. Hussain, Y. Khan, H. Ullah, S. Daud, R. Rahman, R. Iqbal, R.M. Aljowaie, S. Aghayeva, A Combined in Vitro and in Silico Approach of Thiadiazole Based Schiff Base Derivatives as Multipotent Inhibitor: Synthesis, Spectral Analysis, Antidiabetic and Antimicrobial Activity. Results in Chemistry, 9, (2024) 101671. https://doi.org/10.1016/j.rechem.2024.101671

[74] A. Singh, H.P. Gogoi, P. Barman, Comparative Study of palladium(II) Complexes Bearing Tridentate ONS And NNS Schiff Base Ligands: Synthesis, Characterization, DFT calculation, DNA Binding, Bioactivities, Catalytic Activity, And Molecular Docking. Polyhedron, 221, (2022) 115895. https://doi.org/10.1016/j.poly.2022.115895

[75] W. Yang, J. Chen, Z. Peng, G. Wang, Design, Synthesis and Enzymatic Inhibition Evaluation of Novel 4-Hydroxy Pd–C-Ⅲ Derivatives as α-Glucosidase and PTP1B Dual-Target Inhibitors. European Journal of Medicinal Chemistry, 280, (2024) 116938. https://doi.org/10.1016/j.ejmech.2024.116938

[76] P. González, P. Lozano, G. Ros, F. Solano, Hyperglycemia and Oxidative Stress: An Integral, Updated and Critical Overview of their Metabolic Interconnections. International Journal of Molecular Sciences, 24(11), (2023) 9352. https://doi.org/10.3390/ijms24119352

[77] J.S. Bhatti, A. Sehrawat, J. Mishra, I.S. Sidhu, U. Navik, N. Khullar, S. Kumar, G.K. Bhatti, P.H. Reddy, Oxidative Stress in the Pathophysiology of type 2 Diabetes and Related Complications: Current Therapeutics Strategies and Future Perspectives. Free Radical Biology and Medicine, 184, (2022) 114–134. https://doi.org/10.1016/j.freeradbiomed.2022.03.019

[78] B.P. Darwitz, C.J. Genito, L.R. Thurlow, Triple Threat: how Diabetes Results in Worsened Bacterial Infections. Infection and Immunity, 92(9), (2024) e00509–00523. https://doi.org/10.1128/iai.00509-23

Authors Contribution Statement

M. Periyannan: Conceptualization, Methodology, Software, Writing-Original draft preparation, Visualization, Writing-Reviewing and Editing. A. Selvi: Investigation, Formal analysis, Writing -Review & Editing R. Rajavel: Investigation, Writing-Reviewing and Editing Supervision. All authors read and approved the final manuscript.

Funding

The authors declare that no funds, grants or any other support were received during the preparation of this manuscript.

Competing Interests

The authors declare that there are no conflicts of interest regarding the publication of this manuscript.

Data Availability

The data supporting the findings of this study can be obtained from the corresponding author upon reasonable request.

Has this article screened for similarity?

Yes

About the License